Understanding Warm Cloud Aerosol-Cloud Interactions

Alyson R. Douglas

A thesis submitted in partial fulfillment of

the requirements for the degree of

Master of Science

(Atmospheric and Oceanic Sciences)

at the

University of Wisconsin-Madison

August 2017

Thesis Declaration and Approval

I, Alyson R. Douglas, declare that this thesis titled 'Understanding Warm Cloud Aerosol-Cloud Interactions' and the work presented in it are my own.

Alyson R. Douglas		
Author	Signature	Date

I hereby approve and recommend for acceptance this work in partial fulfillment of the requirements for the degree of Master of Science:

Dr. Tristan L'Ecuyer		
Committee Chair	Signature	Date

Dr. Grant Petty		
Faculty Member	Signature	Date

Dr. Matthew Hitchman		
Faculty Member	Signature	Date

Abstract

Understanding Warm Cloud Aerosol-Cloud Interactions

by Alyson R. Douglas

Warm clouds play an important role in Earth's radiative budget, cooling the atmosphere and surface by reflecting shortwave radiation. Increases in biomass burning and other anthropogenic activity could alter Earth's radiative balance through aerosol-cloud-radiation interactions. Unfortunately, modeling and observations have led to little understanding of the expected impacts of aerosols on the cloud's radiative balance, also known as the effective radiative forcing from aerosol-cloud interactions (ERFaci). Aerosol-cloud-radiation interactions, therefore, remain poorly understood, but could have large implications for climate sensitivity. Understanding and decomposing the shortwave warm cloud forcing sensitivity, the efficiency of aerosol to alter a cloud's radiative effect, into meteorological regimes could increase our understanding of the relevant physical processes and help modelers reduce error. This study compares the regime estimated forcing and decomposed forcing sensitivity against regional estimates of the sensitivities, which reveals shortcomings of the regime framework. Using four years of collocated NASA A-Train satellite retrievals along with MERRA reanalysis, warm clouds are separated by environmental regimes using the local stability and free tropospheric humidity. The sensitivities are then further separated by cloud regimes separated by AMSR-E liquid water path. Estimates from regimes are compared to regional estimates of the sensitivities. In the tropics regimes fail to reproduce a negative forcing sensitivity. Regime separation works well

to induce a lower boundary on the forcing sensitivity and its components, however the regional sensitivity estimates are likely to be closer to the truth. Further analysis of the effects of precipitation on aerosol-cloud-radiation interactions, as well as validation of the results against modeled aerosol concentrations are needed.

"All models are wrong; some models are useful.

George Box

To all marine stratocumulus clouds out there acting as Earth's sunblock.

Acknowledgements

There are many people that made this possible.

Firstly, Tristan L'Ecuyer, who provided exemplary guidance.

Second, my wonderful husband, who helped me decode countless Python scripts.

And last but not least, coffee, the greatest gift to mankind, who guided me through the darkest of nights and the longest of days.

Contents

List of Figures

List of Tables

Abbreviations

CCCM	**C**ALIPSO- **C**loudSat- **C**ERES- **M**ODIS
MERRA-2	**M**odern **E**ra **R**etrospective analysis for **R**esearch and **A**pplications Version 2
CPR	**C**loud **P**rofiling **R**adar (aboard CloudSat)
EIS	**E**stimated **I**nverstion **S**trength
ERFaci	**E**ffective **R**adiative **F**orcing due to **a**erosol- **c**loud **i**nteractions
RFaci	**R**adiative **F**orcing from **a**erosol **c**loud **i**nteractions

Symbols

λ	Forcing sensitivity	$\frac{Wm^{-2}}{ln(AI)}$
λ_{RF}	Radiative sensitivity	$\frac{Wm^{-2}}{ln(AI)}$
λ_{CA}	Cloud adjustment sensitivity	$\frac{Wm^{-2}}{ln(AI)}$
Δ	Change from pre-industrial to current times	

Chapter 1

Introduction

1.1 Warm Clouds and Radiation

Warm clouds, low altitude clouds with a cloud top temperature above -5° C, play an important role in Earth's radiative budget, cooling the atmosphere and surface by reflecting shortwave radiation. Marine stratocumulus, a common type of warm cloud, covers a quarter of the Earth's ocean and a tenth of the Earth's land annually averaged, making them the most common type of cloud (Hahn and Warren, 2007). Increases in industrial emissions, biomass burning, and other anthropogenic activity near warm cloud decks could alter Earth's radiative balance through aerosol-cloud-radiation interactions. Unfortunately, despite nearly 40 years of active research, modeling and observations have led to little understanding of the expected impacts of aerosols on cloud radiative properties on

global scales, also known as the effective radiative forcing from aerosol cloud interactions (ERFaci).

The Intergovernmental Panel on Climate Change's (IPCC) fifth report has low confidence in the understanding of changes in radiative forcing due to aerosol-cloud interactions, leading to large margins of error for the potential radiative forcing estimates (Boucher et al., 2013). The current range of estimates from the report are from -1.2 Wm^{-2} to 0 Wm^{-2} of forcing from pre-industrial (1750) to current times. Further uncertainty lies in defining the radiative forcing due to aerosol induced changes in the cloud's thermodynamics and lifetime (adjustments). The RFaci only constitutes half of the clouds reaction to aerosol loading, where aerosol increases the brightness of the cloud. Unlike the RFaci which represents a fast, immediate response to aerosol, cloud adjustments are the long term changes in the physical structure of the cloud. The ERFaci is a combination of RFaci and cloud radiative adjustments. Since the fifth report, efforts have been made to understand ERFaci, however untangling aerosol-cloud-radiation from aerosol-radiation and cloud-radiation interactions is a challenge. A better understanding of these effects is however, essential since the climate sensitivity, a metric of the global sensitivity to a forcing, varies depending on the magnitude and sign of the ERFaci (Randall et al., 2007).

The innovative work of Twomey in 1977 and Albrecht in 1989 laid the groundwork for understanding ERFaci. The albedo effect, or radiative forcing due to aerosol-cloud interactions, is where pollution increases the albedo of the cloud. The RFaci encapsulates the response in the cloud's radiative balance due to an increasing number of small droplets

within the cloud. Aerosols act as cloud condensation nuclei (CCN) within a cloud layer. Twomey theorized an increase of aerosol in a cloud layer leads to more CCN without altering the amount of water inside a cloud, decreasing the mean drop size while increasing the droplet concentration, brightening the cloud (Twomey, 1977).

The lifetime effect, or cloud adjustments, is where the decreased number of cloud droplets in a cloud due to pollution suppresses the time to precipitation, increasing the cloud lifetime and cloud expanse. Cloud adjustments encapsulate the response of a cloud to a suppression of precipitation, leading to a larger expanse throughout a cloud's lifetime and increasing the overall effective radiative forcing of the cloud (Albrecht, 1989). Since Twomey and Albrecht's breakthroughs, little research has been forthcoming about ERFaci.

1.2 Challenges

Observing, modeling, and quantifying ERFaci has proved challenging for researchers. Warm cloud parameterization in models has proven challenging. The key processes that regulate the response and coarse resolution of models lead to large margins of error when simulating aerosol-cloud interactions (Wood et al., 2016). Satellites and field experiments must gather observations on a scale close to the scale of key processes to properly capture all cloud responses. However, it is not possible to observe or explicitly model these scales globally. Models incorrectly use statistics to represent the range of cloud properties, which do not capture the micro- or macrophysical aerosol-cloud interactions

within a cloud layer, resulting in incorrect model estimates of ERFaci. Even if scales of observation can be calibrated to match those of "key processes," identifying how to quantify the key processes, and which are most important to cloud response, remains a challenge. Additionally, all necessary cloud properties and relationships must then be properly parameterized in models and calibrated to observational constraints.

Difficulties in understanding and quantifying key processes remain because cloud processes are sensitive to local meteorology and cloud state, meaning there is significant covariance between cloud and radiative properties due to changing local meteorology and cloud morphology. This covariance and a lack of understanding lead to large intermodel disparities of the ERFaci (Wood et al., 2016). In fact, it has been postulated that the cloud response to aerosol perturbations is controlled by the local meteorology of the cloud's environment, as well as the cloud morphology. The local meteorology and cloud morphology can work to amplify or diminish observed aerosol response, known as buffering. The local meteorology can work to increase the response of the cloud, such as heightening the cloud brightness response, or dampen any micro and/or macrophysical responses. Untangling the cloud response from local meteorology and cloud state could unravel "significant, but regime-specific, responses" (Stevens and Feingold, 2009). Cloud responses, when separated by regime, may reveal regimes where aerosol effects in the cloud are buffered by the cloud system, canceling out any effective changes in ERFaci and adjustments in the cloud thermodynamics.

Is there evidence of regime specific responses? And if a cloud is a buffered system,

how can both the RFaci and adjustments be observed and quantified on global scales if aerosol-cloud-radiation interactions are difficult to constrain? Previous satellite studies have suggested that observations of aerosol, cloud, and radiation information at a high spatial resolution combined with reanalysis of the environment may provide a pathway toward accounting for local meteorology and cloud morphology in global assessments of the ERFaci (Chen et al., 2014, Christensen et al., 2016, Ma et al., 2014). The shortwave RFaci and cloud adjustments determined by recombining the regime specific responses represent observed aerosol-cloud interactions and radiative impact. These approaches have never been rigorously tested to determined how well regime separation works or the degree of separation required to separate all responses.

1.3 Focus of the Study

The focus of this study is to determine the sign and magnitude of the shortwave ERFaci in warm clouds. By only focusing on warm clouds, effects of aerosols on ice nucleation, and the error in satellite observations of ice containing clouds, can be ignored. Warm cloud-aerosol-radiation interactions will be examined, addressing the following questions:

- How large is the shortwave warm cloud effective radiative forcing due to aerosol-cloud interactions?
- Can the two main components of the ERFaci, the albedo effect and cloud adjustments, be quantified individually?
- Does the cloud response depend on regime?

- Are there regional responses not captured by cloud regimes?

1.4 Background

Extensive interest in aerosol-cloud interactions from both the modeling and satellite communities has yielded a rich array of literature, guiding the field. The history of each question will be covered in order to avoid repeating mistakes of other studies and utilize the full potential of satellite observations.

1.4.1 How large is the shortwave warm cloud effective radiative forcing due to aerosol-cloud interactions?

Estimates of the ERFaci vary depending on year studied, cloud type, and data source. The third IPCC assessment report estimated a range from -1.9 to -.5 Wm^{-2} when only estimating the RFaci. The ERFaci is estimated to be in a range from -1.4 to -.5 Wm^{-2} (Penner et al., 2001). Global climate models at the time agreed with the range for both the RFaci (-1.9 to .5 Wm^{-2}) and adjustments (-1.4 to .3 Wm^{-2}) (Lohmann and Feichter, 2005). Unfortunately, advances in modeling and availability of satellite observations since 2001 have not constrained the of estimates or error. The fourth IPCC assessment determined the ERFaci to be between 0 to -2 Wm^{-2} with high uncertainty (Forster et al., 2007). The fifth IPCC assessment report estimated with a low confidence a range from -.95 to .05 Wm^{-2} for the total ERFaci (Boucher et al., 2013).

During the period between the third and fifth assessments, competing signs of the ERFaci have been discovered. The albedo effect (RFaci) may decrease depending on the cloud base height of the aerosol layer within the cloud (Wood, 2007). It has also been suggested aerosol perturbations can lead to a decrease in cloud lifetime (adjustments) by activating an 'evaporation-entrainment feedback' (Small et al., 2009).

A multisensor study in 2008 appraised the warm cloud ERFaci to be -.42 Wm^{-2}, nonetheless "it is cautioned that these results, particularly those dealing with the water path response of clouds, warrant substantial further exploration and confirmation on regional and seasonal scales" (Lebsock et al., 2008). Averaging of the warm cloud ERFaci on a global scale can smooth out annual and regional forcing trends. A collocated satellite study has estimate the ERFaci to be -.44 Wm^{-2}, with error $\pm$ .33 Wm^{-2} , which could almost entirely cancel out the effect on the upper end of error. Neither separation of raining and nonraining scenarios nor stability led to a decrease in error (Chen et al., 2014). A study using the same collocated satellite dataset found the warm cloud ERFaci to be -.20 Wm^{-2} with an error range of .31 Wm^{-2}, which could reverse the sign or double the cooling (Christensen et al., 2016).

Simple relationships do not lead to better estimates of ERFaci nor decrease error. Ma et al. (2014) separated cloudy and clear skies, and used only cloud scenes where aerosol is retrieved near the cloudy scene, but had similar uncertainties with the error and robustness of the signal (Ma et al., 2014). While Chen et al. (2014) used direct measurements of the cloud forcing from CERES, Ma relied on changes in albedo related to changes in

cloud droplet density to estimate a change in forcing. Neither approach led to increased robustness or confidence in ERFaci estimates.

1.4.2 Can the shortwave ERFaci be decomposed into its two components, the RFaci and cloud adjustments?

Decomposing the ERFaci into the RFaci and cloud adjustments has been attempted using satellite observations, field campaigns, and all scales of modeling. Estimates of the magnitude and sign of the two effects continue to show the same substantial error since efforts to understand the individual components began in the early 2000s (Lohmann and Feichter, 2005) (Boucher et al., 2013). Chen et al. 2014 attempted to separate the ERFaci into 'intrinsic' (RFaci) and 'extrinsic' (cloud adjustments) components, however both estimates incurred margins of error that could negate the effects. The 'extrinsic' component particularly may be biased due to "uncertainties that cannot be quantified directly" (Chen et al., 2014). Using models to hold cloud adjustments constant while evaluating the change in RFaci results in covarying relationships between region and time period modeled (Engström et al., 2014). Choosing to ignore cloud adjustments and focus on changes in RFaci have led to reasonable estimates but of only one half of the total effect (McCoy et al., 2017).

Many studies do not attempt to quantify both RFaci and cloud adjustments when using satellite observations and focus only discerning one half, the RFaci, of the ERFaci (Boucher et al., 2013, Christensen et al., 2016, Engström et al., 2014, Kaufman et al.,

2005a, Lebsock et al., 2008, Ma et al., 2014, McCoy et al., 2017, Small et al., 2009, Wang et al., 2012). Relating cloud adjustments to the effective radiative forcing has remained a challenge. Because of that, few studies have attempted to contrast the strength of radiative forcing from aerosol-cloud interactions against cloud adjustments or prove the sum of both components is equal to an observed ERFaci.

There has been success in decomposing the ERFaci using a Newtonian approach. Feingold et al. (2016) identified a method to easily discern trends in the shortwave ERFaci. Yet the authors once again note the strong dependence of aerosol effects, including effects on albedo and lifetime, on local meteorology. The decomposition and phase space used failed to incorporate effects of local meteorology on aerosol-cloud interactions. Further, the cloud morphology and existence of a buffer is not factored into the decomposition (Feingold et al., 2016). Attempts to hold the environmental feedback of cloud-aerosol interactions constant using a kernel method in models could not constrain the impacts of the cloud's microphysical state on aerosol-cloud-radiation interactions (Ghan et al., 2016).

1.4.3 Does the cloud response depend on regime?

There are marked differences in aerosol-cloud-radiation interactions between cloud regimes. While albedo usually shows an increase when aerosol increases, the magnitude of the increase varies by environmental regime. Responses vary between precipitating and non-precipitating clouds; precipitating clouds show a larger albedo effect than non-precipitating (Chen et al., 2014). It has been proposed 'distinct thermodynamic regimes' can modulate

the magnitude and sign of the ERFaci. Stable environments may be less prone to aerosol induced changes due to buffering of the cloud layer, while unstable environments may be more prone to aerosol induced changes due to turbulence and entrainment in the cloud layer (Andersen and Cermak, 2015).

Stability not only influences the amount of mixing within a cloud layer, but the entrainment of free tropospheric air through the cloud top. Entrainment is a key method to the decoupling process, which can lead to variability in an otherwise homogeneous cloud layer (Wood and Bretherton, 2004). Entrainment of high relative humidity air through the cloud top may invigorate the cloud layer, leading to a decoupling of the upper layer from the surface, and embedded cumulus within the warm cloud layer. Embedded cumuli lead to more variability in the cloud in terms of both radiation and cloud properties (Wood, 2012).

Small, regional variation in the ERFaci may be due to the local meteorology of the region rather than aerosol alone (Grandey and Stier, 2010). Wind, stability, relative humidity , etc. can affect not only the cloud layer and response, but affect the aerosol locally. Deepening of the cloud layer occurs as invigoration from aerosol, or entrainment through the cloud top, increases the depth of the marine boundary layer depth, altering the radiative balance of the cloud deck (Altaratz et al., 2014, Wood and Bretherton, 2004). Even small-scale observational studies have trouble separating the effective radiative forcing due to aerosol-cloud interactions from the change in effective radiative forcing due to local meteorology. Separating clouds by environmental regimes, due to the covariability

of aerosol concentration and local meteorology, may constrain estimates of aerosol-cloud interactions (Ghan et al., 2016) Partitioning the effects of local meteorology and cloud morphology from aerosol-cloud interactions is needed to properly parameterize clouds in global climate model (Bony and Dufresne, 2005). Accounting for cloud regimes is the only way to truly constrain the ERFaci.

1.4.4 Are there regional responses not captured by cloud regimes?

Cloud regimes governing response to aerosol perturbations may vary from a global to regional scale. Regime dependent cloud responses have been observed most often over large scales, but discrepancies between regimes may wash out smaller signals (Grandey and Stier, 2010). Small scale affects may not be represented in global regimes. Aerosol type and concentration vary regionally and locally, e.g. a small fire may impact clouds near its plume but not 100km downwind, and without regional separation the effect of the small fire may be dampened in a regime framework.

Using small scale (12km) observations within the regime framework should help represent all effects. Satellite retrieved parameters generally agree with aircraft and station retrieved parameters. Although satellite field of views can be many kilometers of area, satellite observations are suitable to quantify a global cloud susceptibility when years of data are used to analyze trends (Painemal and Zuidema, 2013). Satellite parameters, such as aerosol type and vertical information from the CALIPSO satellite, and cloud parameters and fluxes from the CloudSat satellite, can capture cloud processes in all regions of the Earth on a small scale. Comparing the differences between global estimates from

environmental and cloud state regimes and estimates from regional evaluation at a 15° x 15° scale will reveal what effects global regimes cannot distinguish.

1.5 Summary

The fifth IPCC report has low confidence in the forcing effects from aerosol-cloud interactions (Boucher et al., 2013). Models are unable to correctly parameterize aerosol-cloud interactions, and satellite observations have yet to constrain meteorological and cloud morphological effects enough to yield confidence in observed estimates (Stevens and Feingold, 2009). Thorough analysis of satellite observations constrained within regimes improves our confidence in estimates of the effective radiative forcing due to aerosol-cloud interaction (Christensen et al., 2016). Regional analysis of aerosol-cloud interactions will reveal any shortcomings of the regime framework and convey improvements that can be made to the regime framework. To begin, observations of warm clouds and aerosols are needed.

Chapter 2

Methods

To provide a robust sample to evaluate aerosol-cloud interactions globally, observations from the NASA A-Train satellites from January 1st 2007 to December 30th, 2010 will be used in analysis. Measurements are from instruments aboard the Aqua, CALIPSO, and CloudSat satellites. The A-Train constellation allows for collocated observations from all satellites in the constellation. Global, collocated measurements from four years of data allows for a systematic evaluation of aerosol-cloud interactions in warm clouds.

2.1 Theory

The effective radiative forcing due to aerosol-cloud interactions can be described by the product of the sensitivity of the cloud's radiative effect (CRE) to aerosol and the change in aerosol concentrations since the pre-industrial times.

$$ERFaci = \frac{\delta CRE}{\delta aerosol} * \Delta\ aerosol$$
$$\text{where } \frac{\delta CRE}{\delta aerosol} = \lambda \text{ is the forcing sensitivity} \tag{2.1}$$

Satellite observations of the CRE can be used in equation 2.1 to estimate the sensitivity, from here on referred to as λ. The Clouds and the Earth's Radiant Energy System, or CERES instrument measures the incoming and outgoing radiation of Earth in three channels. Clear sky observations of CERES are approximated using the MODIS collocated cloud fraction to discern clear pixels from cloudy pixels. The monthly mean clear sky shortwave forcing is used to determine the cloud radiative effect (CRE).

CERES shortwave top-of-atmosphere balance for clear scenes (scenes with less than 10% cloud cover) are aggregated over the four year period and gridded by 15°x15°. The monthly mean of each 15° x 15° region is used in equation 2.1 as the clear forcing. The clear sky forcing over the ocean is assumed constant. In regions where no CERES footprint is clear enough to observe a accurate clear sky forcing, the SYN1deg level 3 product from CERES is used to provide "clear-sky filling", which allows for higher confidence radiances in consistently cloudy regions (Loeb, 2014). The CERES cloud forcing is found using the monthly mean clear sky for the region, observed instantaneous all sky flux, and cloud fraction from collocated CloudSat measurements.

The aerosol index from satellite observations will be used as a proxy for aerosol concentration. The Moderate-Resolution Imaging Spectroradiometer, or MODIS, aboard the

Aqua satellite captures information from 36 spectral bands. In the study, MODIS retrieved aerosol optical depth (AOD) and Angstrom exponent are used to calculate the aerosol index (AI). The Angstrom exponent relates the AOD and the wavelength its observed with, allowing the particle size to be inferred if both AOD and the Angstrom exponent are known. The AOD measures the extinction along a path from the MODIS instrument to the ground due to absorption and scattering of aerosols in the path. The product of the AOD and the Angstrom exponent is the AI, a quantity inversely proportional to the size of the aerosol particle. AI has a higher correlation with CCN compared to AOD and is more suitable for aerosol-cloud interaction studies (Dagan et al., 2017). A high AI (2.0) is indicative of aerosol from biomass burning and urban pollution, while a low AI (1.0) is indicative of aerosol from dust and sea salt (Schuster et al., 2006). AI reveals information on both size and extinction properties of the aerosol.

Records of pre-industrial aerosol are scarce; estimates of ΔAI would rely on modeling of the pre-industrial climate to estimate the change in aerosol loading. There is high uncertainty in the accuracy of pre-industrial aerosols. To decrease the error in analysis, all estimates are left as sensitivities in per unit ln(AI) (such as λ) (Carslaw et al., 2017).

2.1.1 Including the Components of the ERFaci

The total radiative effect can be described as the sum of the mean clear sky radiative effect weighted by the fraction of clear sky in a scene and the mean cloud radiative effect weighted by the cloud fraction. The total cloud radiative effect for any scene is the product of the mean CRE and the cloud fraction. Applying the same regression from

2.1 to this definition of CRE, the forcing sensitivity λ can be decomposed into the two components of this new regression.

$$\text{Total Radiative Effect} = \overline{Clear\ Forcing} * (1 - Cloud\ Expanse) + \overline{Cloud\ Forcing} * Cloud\ Expanse$$

from that, $CRE = \overline{Cloud\ Forcing} * Cloud\ Expanse$

and therefore, regressing by aerosol and applying the chain rule

$$\frac{\delta CRE}{\delta aerosol} \approx \frac{\delta Cloud\ Forcing}{\delta aerosol} * \overline{Cloud\ Expanse} + \frac{\delta Cloud\ Expanse}{\delta aerosol} * \overline{Cloud\ Forcing} \tag{2.2}$$

The decomposed forcing sensitivity is the sum of the radiative and cloud adjustment sensitivities. These yield from the main components of the ERFaci, the radiative forcing due to aerosol-cloud interactions (RFaci) and the cloud adjustment effect. To a first degree, the RFaci is the product of the brightening or dimming of the cloud with increased aerosol and the cloud expanse. The cloud adjustments are the product of the swelling or contracting of cloud expanse with increased aerosol and the mean cloud radiative effect. The sensitivities of these describe the propensity of the cloud to brighten or swell due to aerosol loading.

$$
\begin{aligned}
&ERFaci = \frac{\delta CRE}{\delta aerosol} * aerosol = \lambda * aerosol \\
&\frac{\delta CRE}{\delta aerosol} \approx \frac{\delta Cloud\ Forcing}{\delta aerosol} * \overline{Cloud\ Expanse} + \frac{\delta Cloud\ Expanse}{\delta aerosol} * \overline{Cloud\ Forcing} \\
&\text{where } \lambda_{RF} = \frac{\delta Cloud\ Forcing}{\delta aerosol} * \overline{Cloud\ Expanse} \\
&\text{and } \lambda_{CA} = \frac{\delta Cloud\ Expanse}{\delta aerosol} * \overline{Cloud\ Forcing}
\end{aligned}
\tag{2.3}
$$

Note the use of δ in all regressions. The sensitivities in the study are not absolute. All regressions depend on homogeneity in the cloud field and simplifying the RFaci and cloud adjustment terms. The sum of λ_{RF} and λ_{CA} is the decomposed sensitivity.

The first term of the decomposed sensitivity, the RFaci, will be left as a product of the sensitivity and mean cloud expanse, similar to λ. The first term of the decomposition will be referred to as λ_{RF}. The cloud adjustment term will be left as the product of the cloud expanse sensitivity and cloud forcing.

Terms from the decomposition can be found using observations from CloudSat. The cloud shortwave forcing (CSWF) from the CloudSat satellite, which is collocated with other observations from MODIS and CERES, provides information on the brightening or dimming of the cloud and is approximately the cloud forcing term. CloudSat's top of atmosphere forcings, mean solar radiation, and cloud forcings from the 2B-FLXHR-Lidar product are model-derived parameters from measurements utilized to estimate the RFaci. Retrieved vertical to horizontal hydrometeor size are manipulated to derive liquid water and ice contents. Upwelling and downwelling fluxes are then computed using the liquid

water and ice contents in a radiative transfer model. Environmental parameters needed for the radiative transfer model not retrieved by satellites in the A-Train are collected from the European Centre for Medium-Range Weather Forecasting reanalysis model. The surface albedo applied in the radiative transfer model is assumed from historical, seasonal maps. The conditional mean cloud shortwave forcing at the top of the atmosphere is found using the CloudSat retrieved cloud forcing and mean solar radiation. Averages of cloud fraction and conditional mean shortwave forcing are taken on along track averages.

The λ_{RF} assumes the cloud forcing is an adequate proxy of the cloud albedo, which has been successful in other indirect effect studies (Chen et al., 2014). Determining the λ_{RF} using the CSWF is a "top-down" approach. Other studies have chosen to employ a "bottom up" approach to relate the mean effective cloud droplet radius with cloud albedo (Bender et al., 2016). Satellite estimates of cloud droplet effective radius are prone to error, therefore a "top down" approach is more appropriate for the CCCM dataset (Painemal and Zuidema, 2011).

$$\mathrm{CSWF} = \frac{\text{mean solar} \times \sum_{i=1}^{\text{n cloudy pixels}} \dfrac{\text{cloud forcing upwards}}{\text{downwards forcing}}}{\text{n cloudy pixels}} \tag{2.4}$$

The cloud expanse is defined as the number of cloudy pixels from CloudSat over a 12 kilometer swath. The small scale averaging of both the cloud expanse and cloud forcing allow small scale variation to be captured in the decomposition. The mean cloud expanse is dependent on the sample analyzed, and is not the mean cloud expanse on Earth. λ_{CA},

the sensitivity of the cloud expanse to aerosol loading, assumes to a first order that the cloud adjustment effect is the swelling (or contraction) of a cloud in reaction to increased aerosol concentrations.

All sensitivities are based on observed radiances and cloud properties. The effective radiative forcing sensitivity λ, also called the forcing sensitivity, is from CERES, the radiative sensitivity λ_{RF} and cloud adjustment sensitivity λ_{CA} are both from CloudSat. All sensitivities depend on MODIS retrieved AI. The forcing sensitivity is used as a benchmark to compare against the decomposed sensitivity.

$$\begin{aligned} \lambda &= \frac{\delta CRE}{\delta ln(AI)} \approx \lambda_{RF} + \lambda_{CA} \\ \lambda &\approx \frac{\delta CSWF}{\delta ln(AI)} * \overline{CF} + \frac{\delta CF}{\delta ln(AI)} * \overline{CSWF} \end{aligned} \tag{2.5}$$

2.2 Constraining Analysis to Warm Clouds

To homogenize the clouds studied, observations from CloudSat are used to limit our analysis to warm, single layer clouds. The Cloud Profiling Radar (CPR) aboard the CloudSat satellite is a 94-GHz nadir radar which can measure the backscatter of observed clouds (Tanelli et al., 2008). The cloud top height and temperature, the cloud class, and precipitation flag all derived from the CPR 2B-CldClass-Lidar product constrain analysis to single layer warm clouds. Only observations where the cloud top temperature is greater than -5° C and liquid water path, from collocated AMSR-E measurements, less than 700

$\frac{g}{m^2}$ observed over the ocean are used in the analysis. Only 3% of the observations have a liquid water path greater than 700 $\frac{g}{m^2}$, but these can unevenly weigh sensitivity estimates.

2.3 Constructing Cloud Regimes

Environmental cloud regimes are established using estimated inversion strength (EIS) and relative humidity of the free atmosphere. Cloud state regimes are further defined by liquid water path (LWP). The Modern-Era Retrospective analysis for Research and Applications Version 2 (MERRA-2) dataset is used in the study to give information on the local cloud environment. MERRA-2 has almost entirely closed the hydrological cycle of Earth using satellite observations and incorporated effects of aerosols to the Earth's system (Bosilovich et al., 2015). Observational constraints on the Earth's hydrological budget improve confidence in environmental parameters. An atmospheric profile of temperature and relative humidity from MERRA-2 is used in the analysis to calculate the estimated inversion strength (EIS) and the relative humidity at 700 hPa (RH).

The estimated inversion strength (EIS) approximates the stability of the boundary layer using potential temperatures from 700 hPa and the surface combined with the lower tropospheric stability (figure 2.1). Stability is better articulated by the EIS versus the lower tropospheric stability because EIS captures the effects of moisture and the inversion on the stability of the boundary layer. The EIS is well correlated with cloud cover not only in the tropics, as is the case for the lower tropospheric stability (LTS), but the sub-tropics and mid-latitudes as well (Wood and Bretherton, 2006).

Percentiles of EIS and RH partition clouds into cloud regimes. These regimes are then further partitioned by LWP, provided by The Advanced Microwave Scanning Radiometer-EOS a passive microwave instrument aboard the Aqua satellite. For each regime, the forcing sensitivity λ is found using both methods. Constraining regimes by EIS controls variation in cloud layer due to local meteorology, while partitioning by the LWP and RH restricts the variation in the cloud layer due to cloud morphology. Accounting for variation and cloud growth by the local meteorology and cloud morphology constrains covariance between the environment and ERFaci.

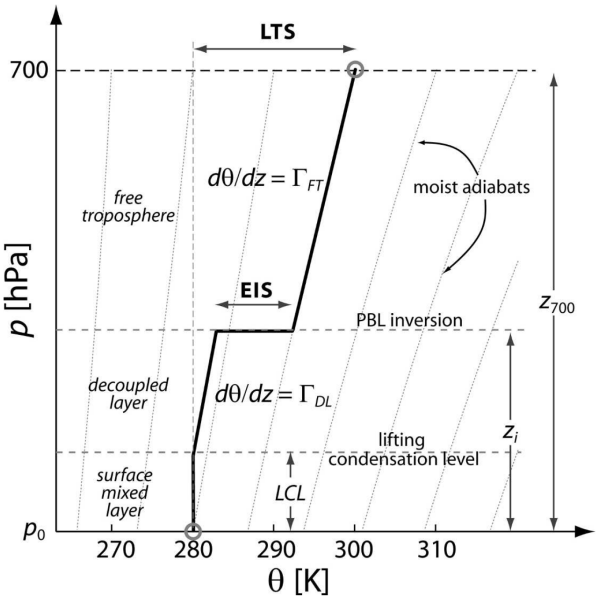

FIGURE 2.1: From Wood and Bretherton (2006), the EIS as a measure of stability in the boundary layer compared to the lower tropospheric stability LTS.

Without regimental constraints the relationship between aerosols and clouds would completely altered by the clouds meteorlogy and state (Gryspeerdt et al., 2016). Cloud adjustments in particular are strongly controlled by both aerosol and the cloud environment. Both can force evaporation or condensation within the cloud (Rosenfeld et al., 2008). The use of cloud regimes allows for an accurate examination of aerosol-cloud interactions and cloud adjustment processes.

2.4 Regional vs. Global

Buffering in the cloud system controlled by regional influences that are not adequately accounted for by single bulk metrics like EIS, RH, or LWP can be identified by regional 15 x 15 estimates. Global evaluations, even when partitioned by environmental and cloud state regimes, may not exhibit all regional effects. While it is known that cloud decks of marine stratocumulus like those studied in (McCoy et al., 2017) show no variation in the sign of all effects, the sign or magnitude of all effects can vary globally. Comparing the regional evaluation to the global estimates can shed light on any missing effects, such as buffering, not captured by the decomposition or properly subset by environmental and cloud state regimes.

2.5 Overview of methods

Satellite observations from CERES, MODIS, and CloudSat are used to estimate the forcing, radiative, and cloud adjustment sensitivities. Observations are constrained within environmental regimes from the MERRA-2 reanalysis estimated inversion strength and relative humidity of the free atmosphere to control the effects of local meteorology. Separation into cloud regimes defined by liquid water path from AMSR-E will then be used to further test the efficacy of regime constraints. Global sensitivities from regimes will be compared against regional sensitivity estimates. If regional sensitivities display behavior not captured by the regimes, regime constraints may not be sufficient to represent all aerosol-cloud interactions seen on Earth.

Chapter 3

Results & Discussion

3.1 Global Regressions

3.1.1 Forcing Sensitivity

It is found in this work that the global and time averaged forcing sensitivity (λ) is estimated to be 13.3 $\frac{\mathrm{Wm}^{-2}}{\ln(\mathrm{AI})}$ (figure 3.1). The effect intensifies for smaller particles, corresponding to a lower ln(AI). As ln(AI) increases, the effect weakens.

Past studies have found the warm cloud ERFaci to be .36, .5, .49, and .4 respectively $\frac{W}{m^2}$ (Chen et al., 2014, Christensen et al., 2016, Gryspeerdt et al., 2017, Schreier et al., 2007). The change in aerosol index due to anthropogenic sources from the pre-industrial to present day would have to be .025 ln(AI) (1.025 AI) globally to reach the same magnitude as others.

A linear regression for all warm clouds observed from 2007 to 2010 violates the core assumption that other forcings are held fixed and does not accurately represent the true warm cloud λ. The time period is too short to remove noise, and the result is likely not representative of the λ for all cloud regimes in all aerosol environments. The use of a single linear regression also limits the ability to account for effect due to the environment. This is important because variation in the effect may signal buffering of the cloud response by the environment.

Correlation between increased CRE and increased ln(AI) does not imply causation. While there is a high correlation between CRE and ln(AI), this can only imply there is a relationship between the two. For all results it is only implied, but not certain, that aerosol loading leads to an increase in cloud radiative effect.

3.1.2 Radiative Forcing Sensitivity

The radiative sensitivity diminishes with increasing ln(AI) corresponding to larger particle sizes (figure 3.2). For the highest ln(AI), however, the sign of λ_{RF} reverses. Higher ln(AI) correspond to the larger amounts of aerosol loading and larger particles. The peak effect is between -3.06 to -2.7 ln(AI). After -2.7 ln(AI), the radiative sensitivity decreases in strength until eventually reversing in sign after -2.1 ln(AI). λ_{RF} shows a binomial relationship with particle size, where the relationship eventually reverses as particle size increases. As a result, the smallest aerosols have the largest radiative forcing effect. The smallest aerosols may most effectively decrease the mean droplet size and brighten the cloud when the aerosol acting as CCN are the smallest.

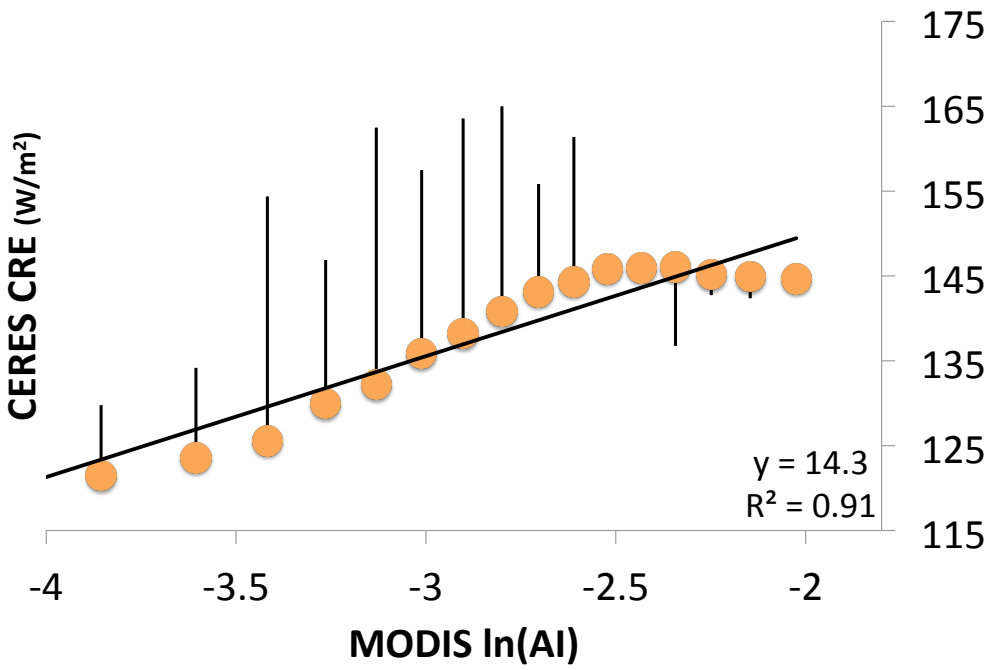

FIGURE 3.1: Global scatter plot of MODIS ln(AI) against CERES CRE $\frac{W}{m^2}$. Each bar represents the strength of the sensitivity at the point.

3.1.3 Cloud Adjustment Sensitivity

λ_{CA} shown in figure 3.3 diminishes at the highest ln(AI), but not to the same degree as the λ_{RF}. The effect peaks for ln(AI) between -2.7 and -2.2, the range of ln(AI) after the radiative sensitivity peaks. Cloud adjustment sensitivity shows a non-linear relationship with the size of the aerosol particle. The effectiveness of aerosol to act as a CCN and alter the droplet size spectrum within the cloud decreases as aerosol size increases.

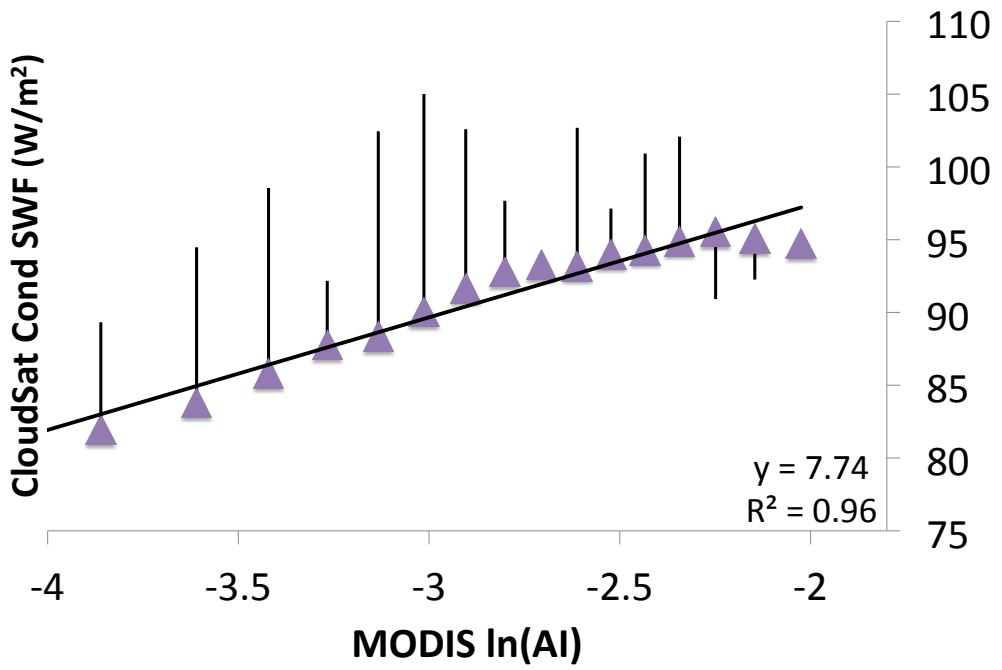

FIGURE 3.2: Global scatter plot of MODIS ln(AI) against CloudSat conditional mean shortwave forcing $\frac{W}{m^2}$. Each bar represents the strength of the λ_{RF} at the point.

The decomposed sensitivity is 9.35 $\frac{\mathrm{Wm}^{-2}}{\ln(\mathrm{AI})}$. The radiative sensitivity comprises 3.56 $\frac{\mathrm{Wm}^{-2}}{\ln(\mathrm{AI})}$, or 40% of the decomposed sensitivity, while the cloud adjustment sensitivity comprises the remaining 5.79 $\frac{\mathrm{Wm}^{-2}}{\ln(\mathrm{AI})}$, or 60%. The decomposed sensitivity is 4.95 $\frac{\mathrm{Wm}^{-2}}{\ln(\mathrm{AI})}$ less than the forcing sensitivity (figure 3.1). The percent difference between the decomposed sensitivity compared to the λ is 35%.

Decomposing the forcing sensitivity in this way allows the inclusion of the cloud adjustment sensitivity, which may not be captured by a single linear regression of MODIS

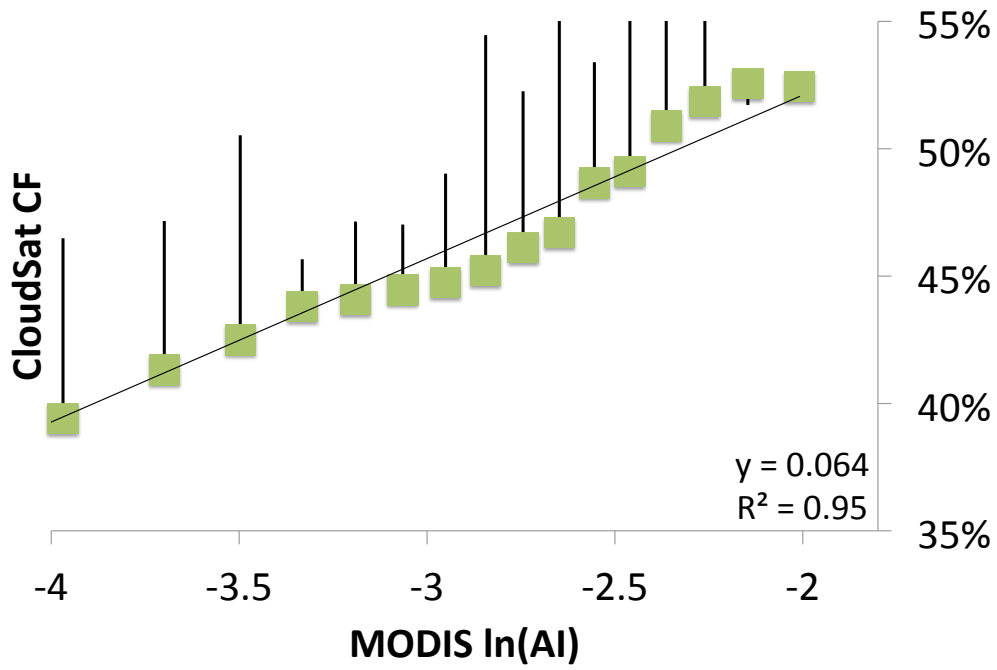

FIGURE 3.3: Global scatter plot of MODIS ln(AI) against CloudSat along track cloud fraction. Each bar represents the strength of the cloud adjustment sensitivity at the point.

ln(AI) against the CERES CRE (λ). λ_{CA} the main effect represented by the modified cloud extent, directly connects long term consequences of aerosol loading in the cloud layer (i.e. increased lifetime) with the cloud's radiative effect. Without the inclusion of the λ_{CA}, the forcing sensitivity would be underestimated, and depend solely on the λ_{RF} (figure 2).

The response of cloud extent to aerosol loading has been discussed in recent literature. Previous studies have found both larger, smaller, and oscillating between larger to smaller

cloud extents due to aerosol. In our results, the λ_{CA} is found to lead to cooling due to increased cloud extent for all aerosol scenarios except for ln(AI) greater than -1.8. Our results agree with previous modeling studies which have estimated λ_{CA} and the λ_{RF} are of comparable magnitude (Lohmann and Feichter, 2005).

Unlike the λ_{CA}, the λ_{RF} is strongest for lower aerosol environments and the efficiency greatly decreased with aerosol loading. The aerosol environment and activation of aerosol control the strength of the radiative sensitivity (Koren et al. (2014), Chandrakar et al. (2016), Sandu et al. (2008),Stevens and Seifert (2008).)

The decomposed sensitivity is 35% less than the forcing sensitivity, however the forcing sensitivity may not capture variation in the effect. Mauger and Norris (2007) estimated a single linear regression method may overestimate the effect by as much as 30%. Likewise, λ_{RF} from a single global linear regression using MODIS AI may underestimate the sensitivity by as much as 30% (Carslaw et al., 2013). Interestingly, if λ_{RF} is underestimated by a global linear regression, the difference between the overestimated forcing sensitivity and the underestimated decomposed sensitivity would decrease to 4%.

The use of a single linear regression does not allow for regional variation in response to be incorporated into estimates. Variation in each independent component, λ_{RF} and λ_{CA}, can then be understood as a function of AI. The inclusion of variation by using two terms dampened the magnitude relative to the first estimate (figure 3.1), however a single global regression overestimates the effect. Aerosol-cloud interactions depend on the local meteorology, which modulates the magnitude and sign of each component.

Although the decomposition does allow for each component to vary in magnitude, a global linear regression prevents distinguishing influences due to local meteorology. Local meteorology, like the boundary layer stability and free atmosphere RH, modulate aerosol-cloud interactions by acting as a buffer to the system. Th sensitivities diagnosed from global linear regressions should be held as an upper limit of the effects. As variation is included within estimates of the forcing and decomposed sensitivities, whether through cloud regimes or diagnosing on different scales, estimates should decline towards the actual value.

3.2 Accounting for environmental controls

3.2.1 Forcing Sensitivity

The magnitude of λ varies significantly between the cloud regimes of estimated inversion strength (EIS) and relative humidity in the free atmosphere (RH) (figure 3.4). The forcing sensitivity when evaluated within each regime and weighted by frequency is 3.1 $\frac{\mathrm{Wm}^{-2}}{\ln(\mathrm{AI})}$. The largest effect is observed in the most humid and most stable cloud regime. The smallest effect is for the driest and least stable cloud regimes. The highest RH regimes, i.e. those with RH greater than 55%, show a strong dependence on stability. For the least stable regimes, increasing RH has an negligible effect. For the most stable regimes,however, increasing RH can double the effect.

Evaluating the forcing sensitivity in an environmental regime framework allows variation between cloud regimes to be compared. Cloud regimes help identify environments acting

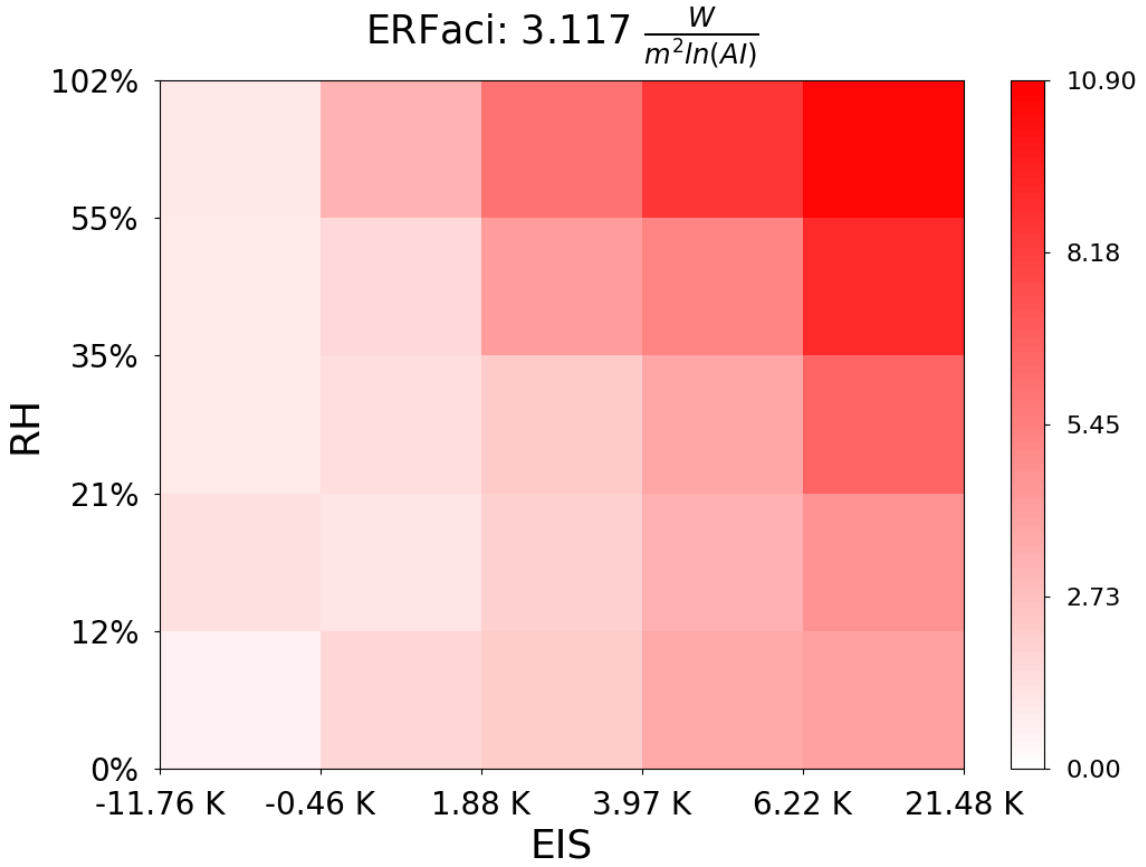

FIGURE 3.4: The forcing sensitivity found within global regimes of RH and EIS. Cloud regimes are unweighted.

as a buffer to inhibit aerosol-cloud interactions. For example, unstable regimes may be acting as a buffer to aerosol-cloud interactions. These regimes show the smallest effect compared to stable, moist regimes. The unstable regimes may alter the evaporation-entrainment feedback of the cloud, resulting in a reduced sensitivity (Jiang et al., 2006).

The largest aerosol effects observed are in the most humid and stable environments. The moist free atmosphere may support high amounts of cloud top entrainment. Conversely, if the moisture in the free atmosphere is not a result of turbulent mixing between the cloud and free atmosphere, then entrained moist free atmosphere air can invigorate the

cloud layer. However, the high stability of the boundary layer would limit cloud top entrainment, preventing the free atmosphere from drying out the cloud layer. The moist, stable environment allows for the greatest activation of aerosol, heightening the effect. Results suggest that stable environments with intensive mixing within the cloud layer may lead to a greater sensitivity, enhancing the effect.

When the weighted sum of effects is computed, it more accurately holds the cloud constant. Using the regression assumes the cloud to be held approximately constant with respect to the environment and cloud state; incorporating regimes allows enforces this assumption. Further incorporation of cloud state regimes should more accurately control for variation assumed in the methods to be constant.

3.2.2 Radiative and Cloud Adjustment Sensitivities

The radiative sensitivity comprises 2.009 $\frac{\mathrm{Wm}^{-2}}{\ln(\mathrm{AI})}$, or 53%, of the decomposed sensitivity (figure 3.5). λ_{RF} shows similar patterns to λ (figure 3.4). The maximum effect is for the moistest and most stable regimes. Low stability regimes show a decreased effect with a moist FA, while high stability regimes show an increased effect for as the free atmosphere moistens. As a result, the highest RH regimes show a strong dependence on stability.

The contribution of λ_{RF} to the decomposed sensitivity increased when evaluated within environmental regimes. λ_{RF} shows signs of buffering by the environment in unstable regimes, similar to the forcing sensitivity, where the effect is dampened and independent of the RH. The radiative sensitivity increases as RH and stability increases, signaling

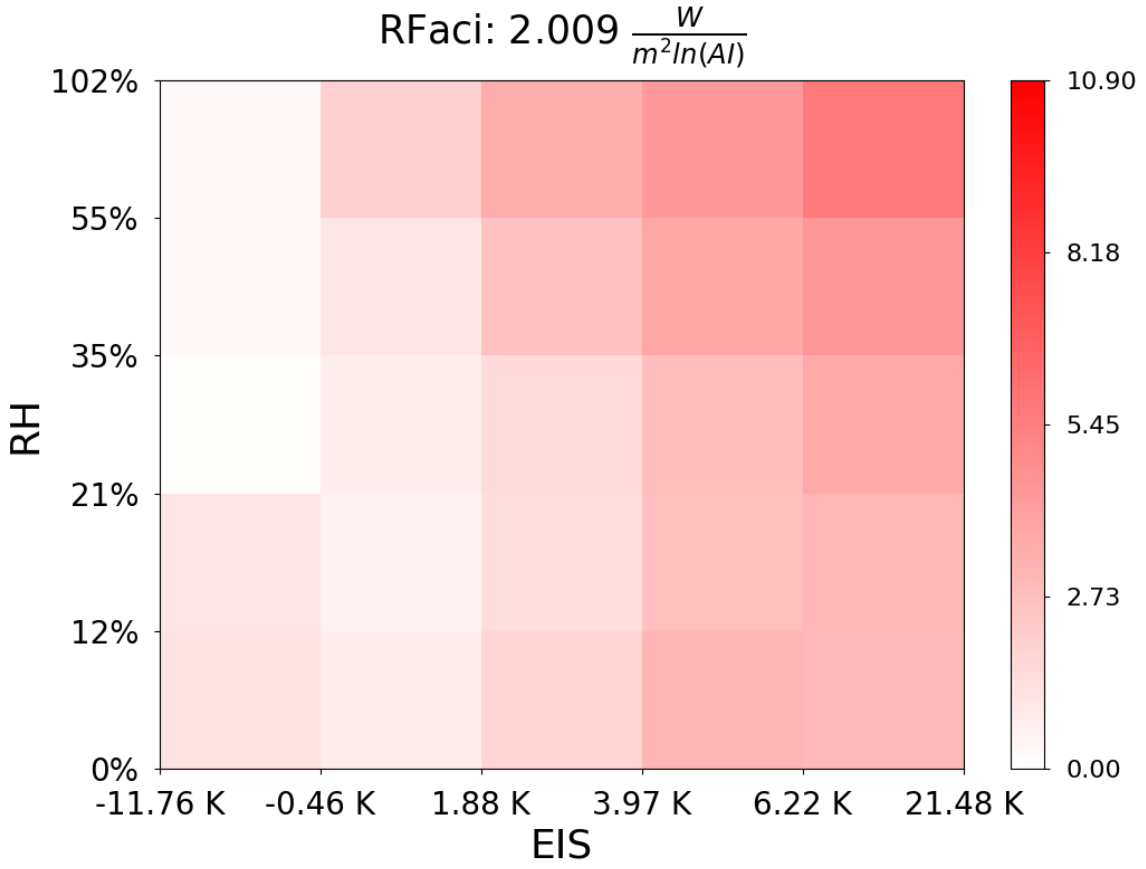

FIGURE 3.5: The radiative sensitivity found within global regimes of RH and EIS.

the CSWF (and cloud albedo) require stable environments with high rates of cloud top entrainment to maximize the λ_{RF}. This suggests stable environments are most conducive to maximizing activation of aerosol, leading to the greatest radiative sensitivity.

λ_{CA} contribute 47% or .802 $\frac{\mathrm{Wm}^{-2}}{\mathrm{ln(AI)}}$ of the decomposed sensitivity (figure 3.7). Regimes with low stability and moisture did not have a a sufficiently high correlation to be included the in analysis. In these regimes the decomposed sensitivity completely depends on the radiative sensitivity. Like λ_{RF}, the cloud adjustment effect strengthens in stable environments. The cloud adjustment sensitivity does not exhibit the same enhancement

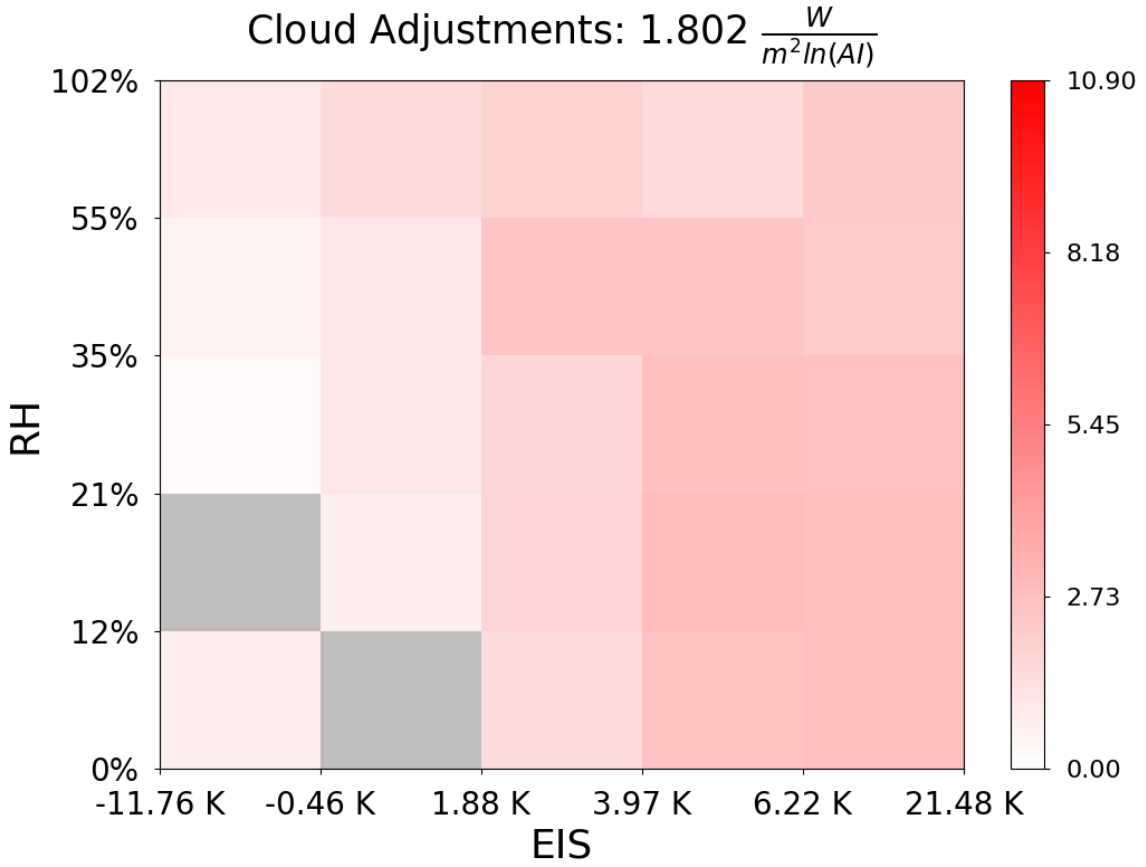

FIGURE 3.6: The cloud adjustment sensitivity found within global regimes of RH and EIS.

for moist free atmosphere in stable environments; suggesting the effect in stable regimes is independent of RH.

Within the highest humidity regime, the effect increases as stability increases. The cloud adjustment process may be undergoing two counteracting processes in moist regimes. High humidity in the FA may serve to accelerate precipitation in warm clouds (Ackerman et al., 2004), while stability increases the activation of aerosol, decreasing the mean droplet size but also increasing the time to precipitation. The ability of the cloud to precipitate likely impacts cloud adjustment sensitivity due to aerosol-cloud interactions.

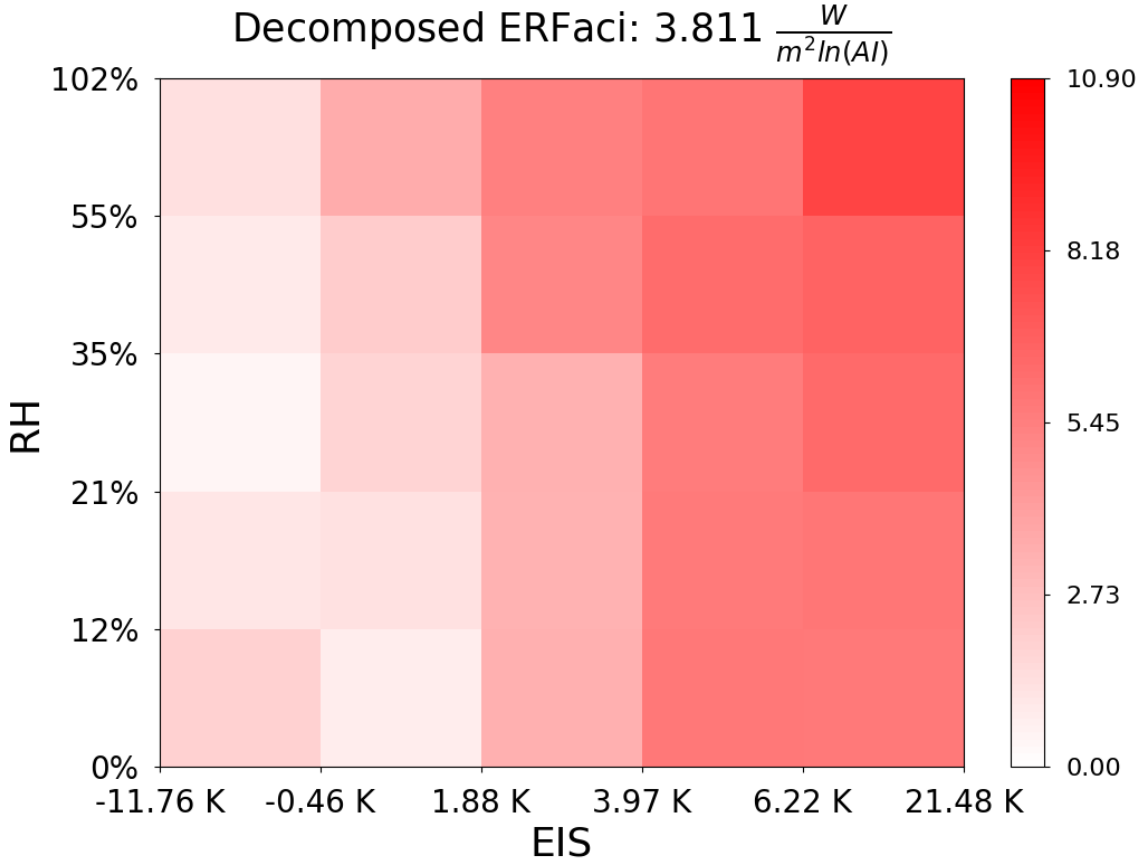

FIGURE 3.7: The decomposed sensitivity found within global regimes of RH and EIS. Cloud regimes are unweighted.

3.2.3 Decomposed Sensitivity

Evaluating λ_{RF} and λ_{CA} within each cloud regime, the decomposed sensitivity is estimated to be 3.811 $\frac{\mathrm{Wm}^{-2}}{\ln(\mathrm{AI})}$ (figure 3.5). The percent difference between the forcing and the decomposed sensitivities is -22%. The decomposed sensitivity displays similar patterns of effect as λ (figure 3.4). The largest effect is again for the most humid and stable regime. The maximum magnitude is 3 $\frac{\mathrm{Wm}^{-2}}{\ln(\mathrm{AI})}$ less than the forcing sensitivity from figure 3.4. Although λ has a greater maximum effect, the decomposed sensitivity indicates a greater

number of stable environmental regimes with a high (7 $\frac{\mathrm{Wm}^{-2}}{\ln(\mathrm{AI})}$) magnitude.

The difference between the two methods of assessing a sensitivity decreased from 35% to 22% with the inclusion of environmental regimes. Environmental regimes allow for better accounting of buffering mechanisms in both methods of evaluating the sensitivity. The decomposed sensitivity shows the same signs of buffering in unstable regimes as λ. For neutral to stable regimes, the decomposed sensitivity shows greater cooling. Assessment of the forcing sensitivity and cloud adjustment sensitivity can help determine the component responsible for the dampening or enhancement of the decomposed sensitivity.

3.2.4 Incorporating Cloud State Regimes

The partial derivative decomposition outlined in 2.4 also requires accounting for cloud morphology when computing the mean CSWF and CF. Indeed, the albedo effect outlined by Twomey in 1977 explicitly applies only to clouds with a fixed liquid water path. Variation of LWP within environmental regimes may lead to contrasting effects due to cloud morphology. To further investigate the effects of cloud morphology, λ is evaluated within cloud regimes of LWP, EIS and RH. The total forcing sensitivity from the summed regimes is 3.186 $\frac{\mathrm{Wm}^{-2}}{\ln(\mathrm{AI})}$ (figure 3.8). The higher LWP regimes show less organization than the lowest LWP regimes. In low LWP regimes, the greatest sensitivities are organized in the high stability and high RH regimes.

Above .2 $\frac{kg}{m^2}$, the contribution from the LWP regime is negligible. The effect for higher LWP regimes is dampened due to weighting, although higher LWP regimes show a higher

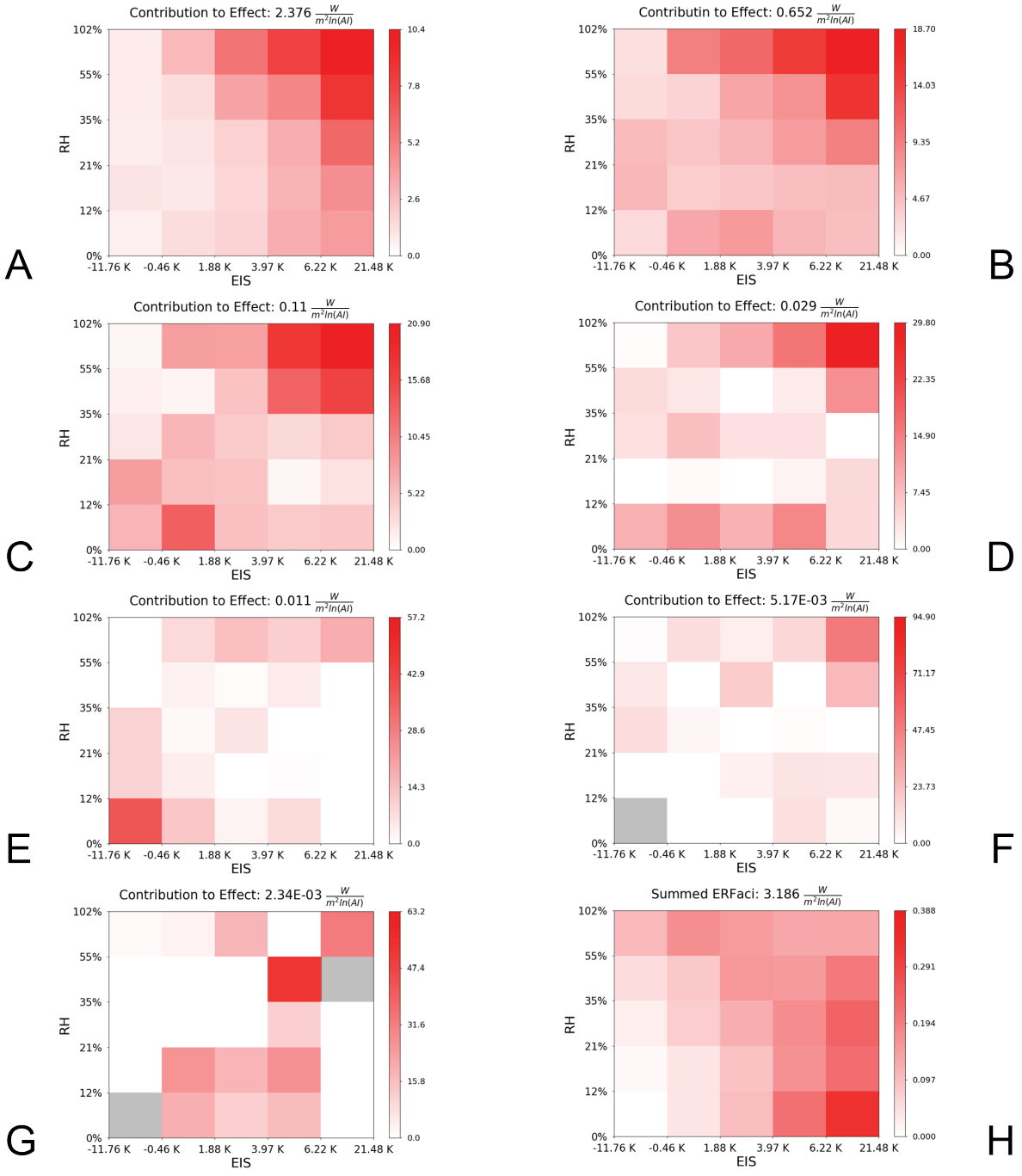

FIGURE 3.8: The forcing sensitivity found within global regimes of RH and EIS separated further by LWP in $\frac{kg}{m^2}$ A) .02 to .1 B) .1 to .2 C) .2 to .3 D) .3 to .4 E) .4 to .5 F) .5 to .6 G) .6 to .7 H) the weighted sum of λ within each regime of RH and EIS. *Note the colorbars are not consistent between the plots.

magnitude maximum than lower LWP regimes. The maximum forcing for LWP regimes above .4 $\frac{kg}{m^2}$ is always above 55 $\frac{\mathrm{Wm}^{-2}}{\ln(\mathrm{AI})}$. Suggesting that the maximum effect always occurs in a most moist, stable regime. As stability and relative humidity decrease, the effect decreases in all LWP regimes. The unweighted effect increases as a function of LWP, confirming the cloud morphology plays a role in modulating the sensitivity.

Separating by regimes of LWP allows influences of cloud liquid water, to be held relatively constant. The forcing sensitivity increases when LWP is constrained is to 3.186 $\frac{\mathrm{Wm}^{-2}}{\ln(\mathrm{AI})}$, .069 $\frac{\mathrm{Wm}^{-2}}{\ln(\mathrm{AI})}$ greater than without LWP regime limits. The largest contribution is from the thinnest clouds, with an LWP less than .2 $\frac{kg}{m^2}$. These results are consistent with field campaigns that have shown even the thinnest clouds may have a large forcing overall due to their abundance (Hirsch et al., 2017). However, these results also demonstrate that the sensitivity to aerosol depends on LWP. The dependence of the forcing sensitivity on LWP constraints, and the dominance of low LWP clouds, implies the relationship between LWP and aerosol-cloud interactions must be parameterized in models in order to constrain covarying effects (Quaas et al., 2009). Models must accurately simulate LWP in order to faithfully represent the warm cloud ERFaci (Wang et al., 2011). Model parameterizations have improved the representation of warm cloud moisture fluxes, which strongly control low cloud variance (Guo et al., 2014). Confidence in estimates of the ERFaci depends on cloud paramerizations continuing to improve.

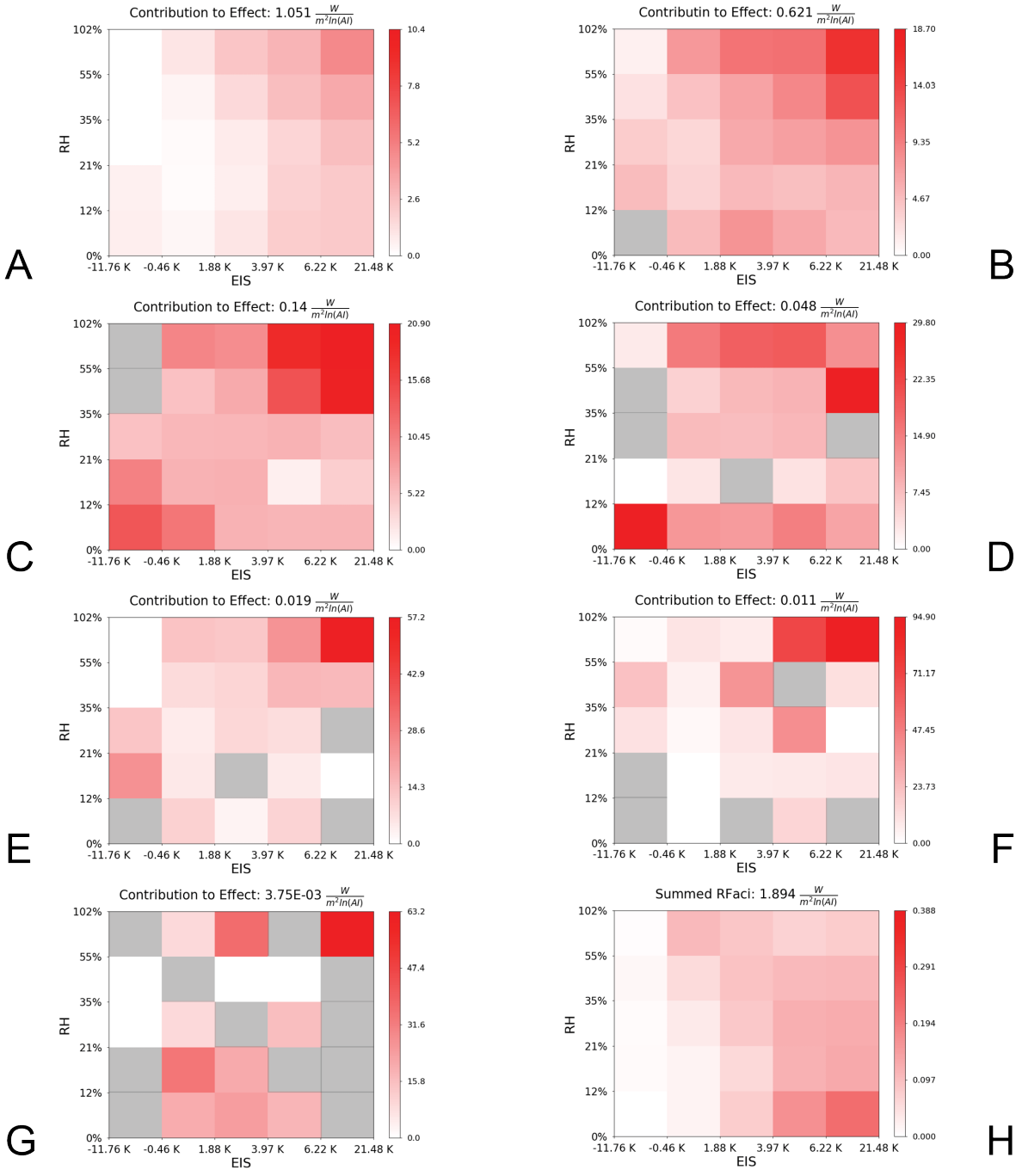

FIGURE 3.9: The radiative sensitivity found within global regimes of RH and EIS separated further by LWP in $\frac{kg}{m^2}$ A) .02 to .1 B) .1 to .2 C) .2 to .3 D) .3 to .4 E) .4 to .5 F) .5 to .6 G) .6 to .7 H) the weighted sum of λ_{RF} within each regime of RH and EIS. *Note the colorbars are not consistent between the plots. Grey regimes denote cloud regimes where the correlation between CRE and ln(AI) is statistically insignificant.

3.2.4.1 Radiative and Cloud Adjustment Sensitivities

The radiative sensitivity, when summed by cloud regimes of LWP, EIS, and RH, contributes 1.894 $\frac{\mathrm{Wm}^{-2}}{\ln(\mathrm{AI})}$, or 60% of the decomposed sensitivity. The largest contribution, as shown in figure 3.10, is from the lowest two LWP regimes, similar in pattern to λ from section 3.3.1. λ_{RF} displays the smallest magnitude response in the lowest LWP regimes. The maximum effect is only 10.4 $\frac{\mathrm{Wm}^{-2}}{\ln(\mathrm{AI})}$ for the lowest LWP regime, compared to 20.9 $\frac{\mathrm{Wm}^{-2}}{\ln(\mathrm{AI})}$ for LWPs between .2 and .3 $\frac{kg}{m^2}$. The effect increases significantly as LWP increases. Grey regimes denote cloud regimes where the correlation between CRE and ln(AI) is statistically insignificant.

The radiative sensitivity shows a stronger effect for high stability and high relative humidity regimes compared to λ_{CA}. The magnitude in all regimes of LWP of λ_{RF} is greater than λ_{CA}. When weighted by occurrence, however, the regimes where the radiative sensitivity is maximized occur less than 3% of the time. If the regimes shift in the future towards higher relative humidity, the λ_{RF} will rapidly increase.

The effect diminishes for higher liquid water paths, most likely due to the nature of the hypothesis behind the effect. Twomey estimated the albedo would increase if cloud liquid water is held constant. Higher liquid water paths are more likely to precipitate, decreasing the efficiency of the cloud to increase droplet concentration and decrease droplet size. The effect Twomey hypothesized is truly only possible in models since liquid water will increase due to aerosol-cloud interactions, violating the main assumption of the effect.

3.2.4.2 Decomposed Sensitivity

λ_{CA}, when summed by regimes of LWP, EIS, and RH, contributes 1.244 $\frac{\mathrm{Wm}^{-2}}{\ln(\mathrm{AI})}$, or 40% to the decomposed sensitivity (figure 3.11). The cloud adjustment sensitivity has a much smaller magnitude effect consistent across all regimes of LWP, RH, and EIS. The number of regimes lacking statistically significant regressions increases as the LWP increases. Unlike λ_{RF} and λ (figures 3.10 and 3.9),λ_{CA} does not vary between regimes.

In thinner clouds, aerosol loading increases the number of CCN in the cloud, invigorating the cloud rapidly (Christensen and Stephens, 2011). The opposite is true in thicker clouds with higher LWPs. Thicker clouds adjust the cloud morphology, diminishing the efficiency of aerosol to alter precipitation processes and inhibiting the cloud growth precipitation suppression process (Goren and Rosenfeld, 2015). Susceptibility of the cloud may depend not only on LWP, but on the initial cloud height and thickness (Wood, 2007). The initial susceptibility has implications on the ability of aerosol to alter precipitation within the cloud. If the cloud thickens, more aerosol is required to delay precipitation, while if the cloud thins, less aerosol is needed to delay collision coalescence (Goren and Rosenfeld, 2015). The local meteorology, especially RH in the free atmosphere, can work to buffer or invigorate the cloud's response (Lu and Seinfeld, 2005), (Ackerman et al., 2004). Future work should explore the linkages among the efficiency of aerosol to alter precipitation, the effects altering precipitation has on the cloud state and the cloud's radiative forcing.

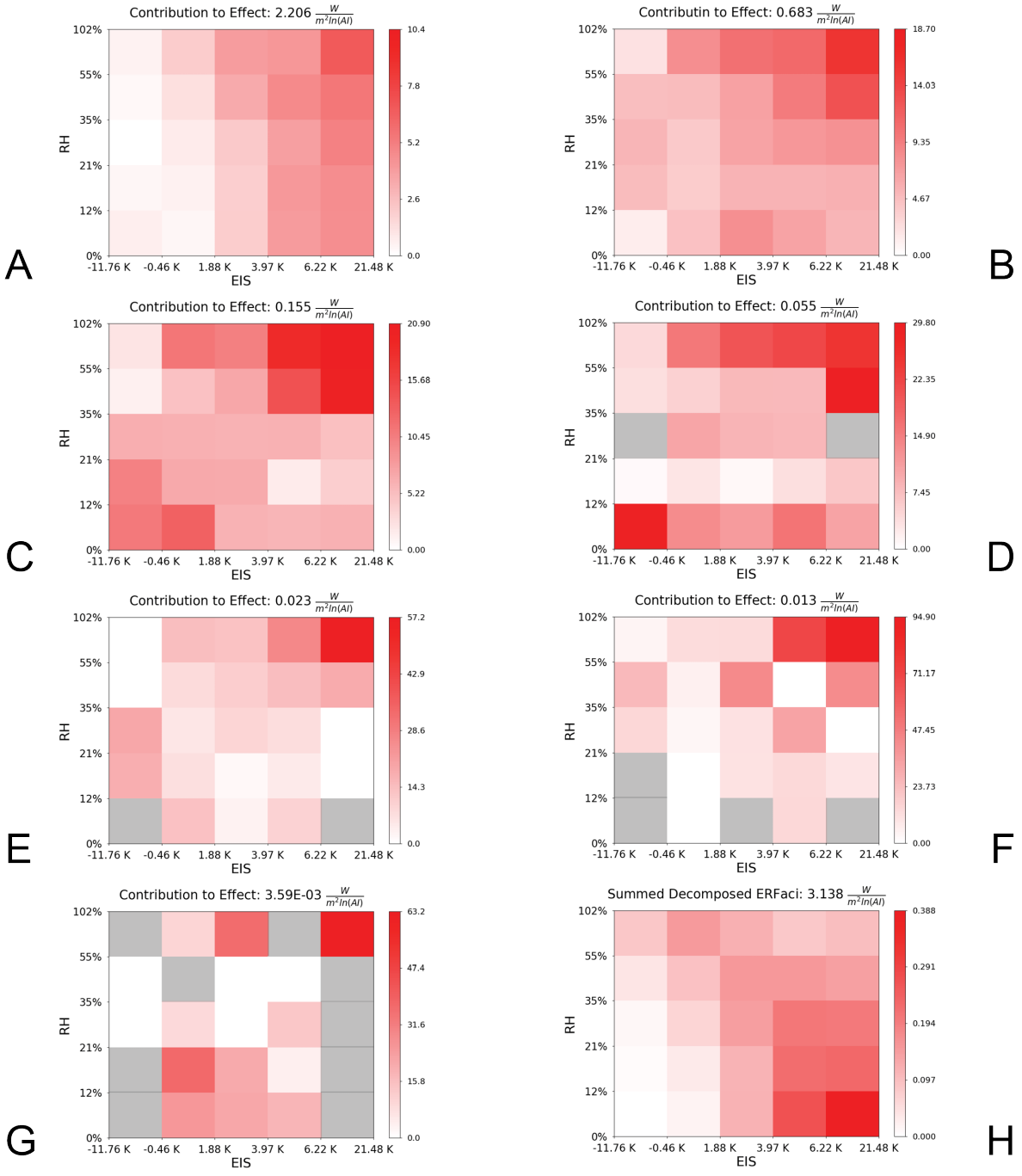

FIGURE 3.10: The decomposed sensitivity found within global regimes of RH and EIS separated further by LWP in $\frac{kg}{m^2}$ A) .02 to .1 B) .1 to .2 C) .2 to .3 D) .3 to .4 E) .4 to .5 F) .5 to .6 G) .6 to .7 H) the weighted sum of the decomposed sensitivity within each regime of RH and EIS. *Note the colorbars are not consistent between the plots.

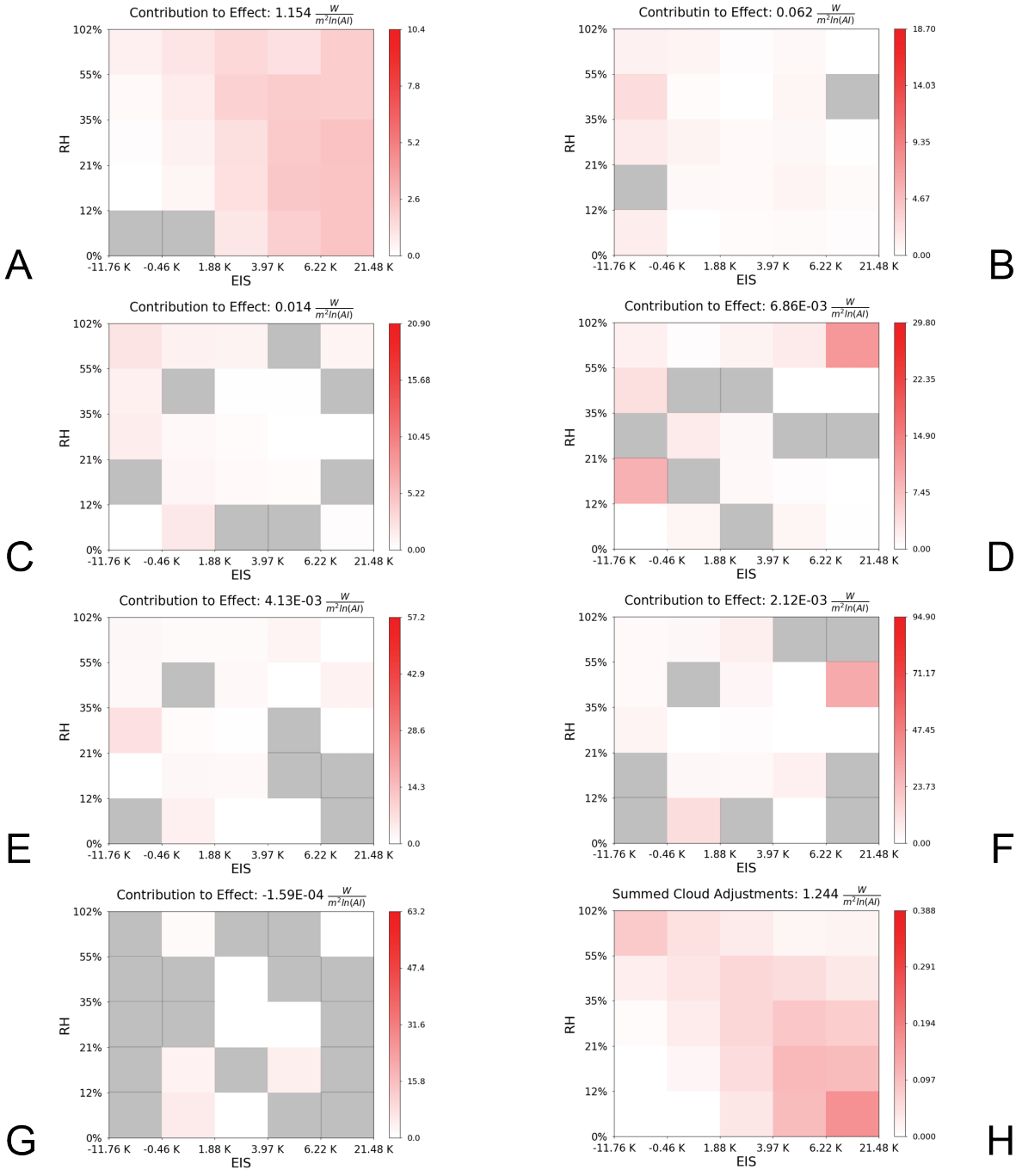

FIGURE 3.11: Cloud adjustment sensitivity found within global regimes of RH and EIS separated further by LWP in $\frac{kg}{m^2}$ A) .02 to .1 B) .1 to .2 C) .2 to .3 D) .3 to .4 E) .4 to .5 F) .5 to .6 G) .6 to .7 H) the weighted sum of λ_{CA} within each regime of RH and EIS. *Note the colorbars are not consistent between the plots. Grey regimes denote cloud regimes where the correlation between CRE and ln(AI) is statistically insignificant.

3.2.4.3 Decomposed Sensitivity

The weighted sum within cloud regimes of LWP, EIS, and RH of the decomposed sensitivity is 3.148 $\frac{\mathrm{Wm}^{-2}}{\ln(\mathrm{AI})}$ (Figure 3.9). A majority of the forcing comes from the two lowest LWP regimes, from .02 to .2 $\frac{kg}{m^2}$. Separating cloud regimes further by LWP has converged the sensitivities. The percent difference between the two sensitivities has decreased with additional regime separation to 1.5%.

The decomposed sensitivity has similar contributions by each LWP regime as λ from figure 3.8. The lowest LWP regime, from .02 to .1 $\frac{kg}{m^2}$, contributes 2.206 $\frac{\mathrm{Wm}^{-2}}{\ln(\mathrm{AI})}$ to the decomposed sensitivity, compared to 2.376 $\frac{\mathrm{Wm}^{-2}}{\ln(\mathrm{AI})}$ to the forcing sensitivity. The distribution of the magnitude of effect is similar between figures 3.8 and 3.9. The decomposed shows the same signature of maximum magnitude cloud regimes occurring in high humidity, stable regimes for most LWPs. The number of statistically insignificant regimes increases as LWP increases for decomposed sensitivity.

3.2.5 Regime Frequency

3.2.5.1 Environmental Regimes

Clouds are most likely to be observed in moist, unstable regimes or dry, stable regimes (figure 3.12). In moist regimes, clouds are more likely to be stable while in dry regimes, clouds are more likely to be unstable. As clouds increase in stability, the average RH

decreases. The maximum effect for the forcing sensitivity (figure 3.8) and the radiative sensitivity (figure 3.10) occurs in stable, moist regimes which are the least likely to occur.

It is interesting to note that the most frequent environmental regimes do not coincide with environmental regimes where the maximum effect occurs. Thus the dependence of aerosol effects on environmental regime has implications for aerosol-cloud interactions in a future climate that extend beyond changes in aerosol concentrations themselves. If the free atmosphere moistens in the future, cooling due to ERFaci may increase through an increased radiative sensitivity. λ_{RF} is maximized in stable, moist environments. The cloud adjustment effect would likely remain unchanged if the FA moistens because it is almost constant with RH for stable regimes. Overall, a moist FA would lead to more cooling.

If the average stability decreases, and the RH remains unchanged, the all sensitivities would all decrease in strength. The radiative sensitivity would experience a larger decrease than cloud adjustment sensitivity due to λ_{RF}'s dependence on cloud regime. λ_{CA} shows a slight decrease for less stable regimes, however λ_{RF} decreases significantly as the environment becomes unstable. With a decrease in stability, the forcing sensitivity would decrease to the same magnitude to λ_{RF}. A change in the environmental stability modifying the λ would most likely be attributed to a decreased λ_{RF}.

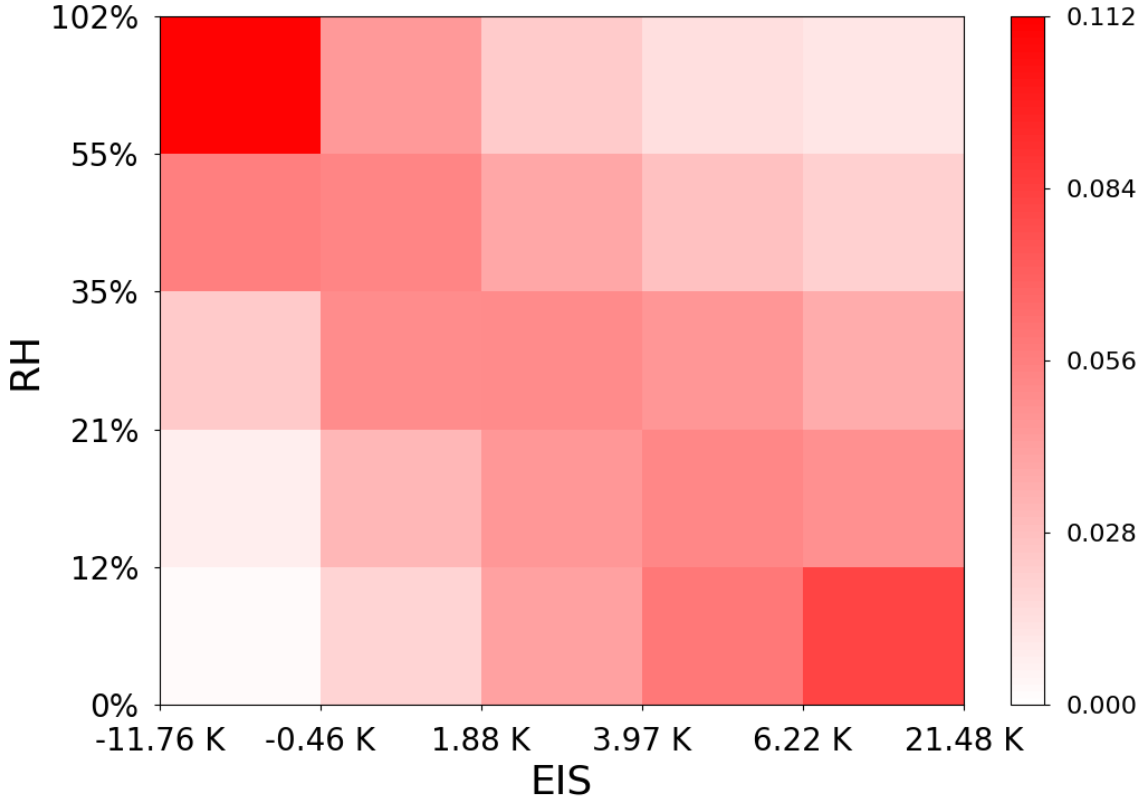

FIGURE 3.12: Frequency of occurrence in % for each environmental regime for .02 to .7 $\frac{kg}{m^2}$.

3.2.5.2 Cloud Regimes

Throughout regimes of LWP, clouds are most likely to occur in the moistest and least stable or driest and most stable regimes. As LWP increases, the frequency of clouds occurring in dry and stable regimes decreases. In the highest LWP regime, almost all clouds are found in the moistest and least stable regime. The lowest LWP cloud regimes, with a LWP less than .3 $\frac{kg}{m^2}$, show a bimodal distribution of clouds, with the highest frequencies grouped in opposite environmental regimes. As the LWP increases, the bimodality of

the frequency decreases, until .6 $\frac{kg}{m^2}$ where the frequencies are clustered solely around the highest humidity, least stable environmental regime.

As mentioned before, the lowest LWP regime contributes the highest number of occurrences globally. Thin, liquid clouds, like trade cumulus and thin marine stratocumulus, dominate warm cloud types. If in the future, the average LWP of warm clouds increases, cooling would increase due to an increased forcing and radiative sensitivity. However, in order to significantly alter the distribution and force a mean regime shift, the frequency of higher LWP clouds would have to greatly increase. Future climates are more likely to see an environmental regime shift than a cloud regime shift because of the almost complete dominance of low LWP clouds.

3.3 Effects of Unknown Regional Influences

Bulk metrics like those employed in 3.1 may not constrain environmental impacts on the cloud, as demonstrated in 3.2. Incorporating environmental and cloud regimes does account for buffering by local meteorology and the cloud state, but may artificially dampen the signal. To test the efficacy of regime separation, the sensitivities are evaluated regionally. Any effects not displayed in environmental or cloud regime separation may signify regime separation does not always capture all effects.

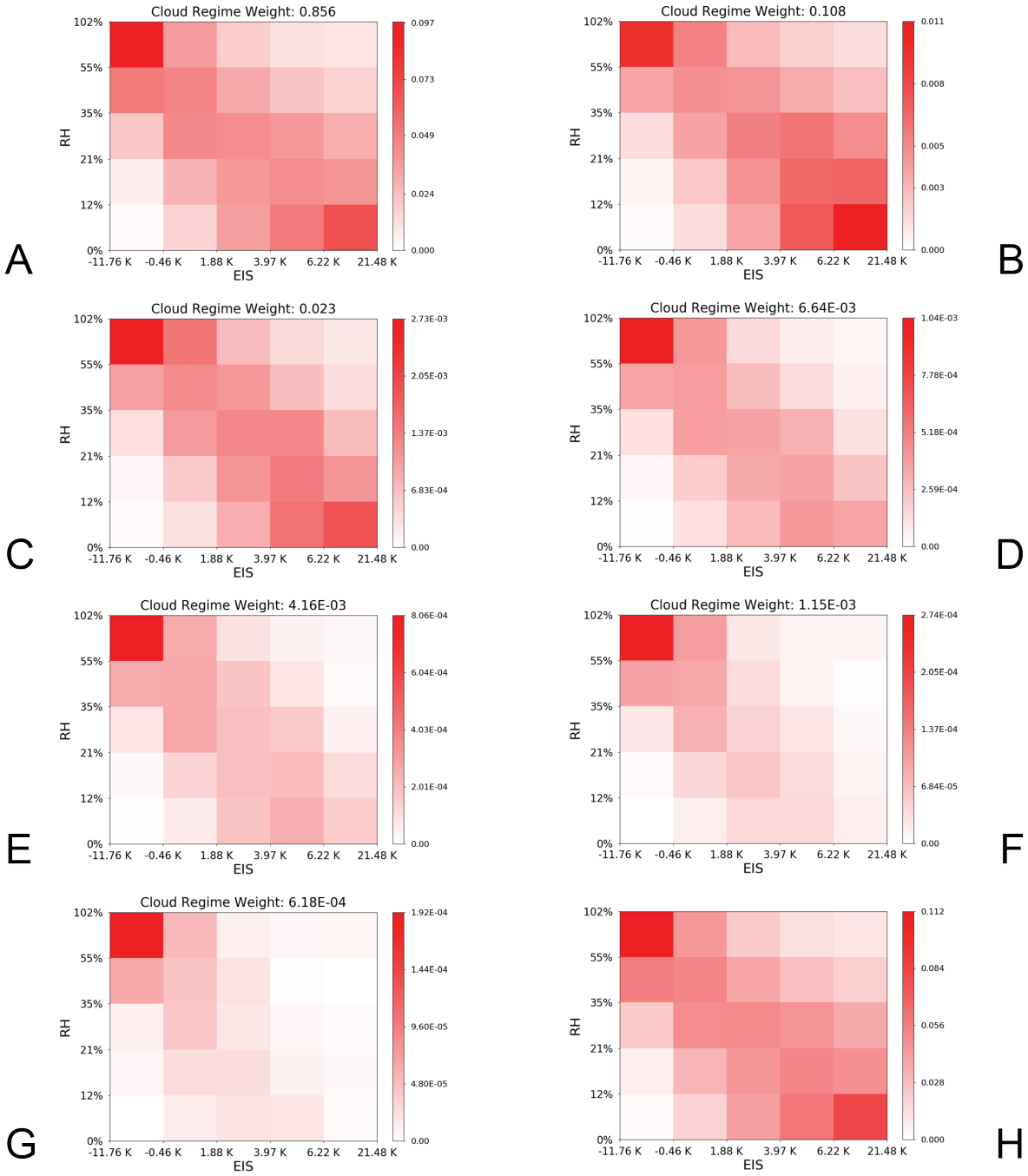

FIGURE 3.13: Frequency of occurrence in % for each environmental regime within cloud regimes of LWP separated by A) .02 to .1 B) .1 to .2 C) .2 to .3 D) .3 to .4 E) .4 to .5 F) .5 to .6 G) .6 to .7 H) $\frac{kg}{m^2}$

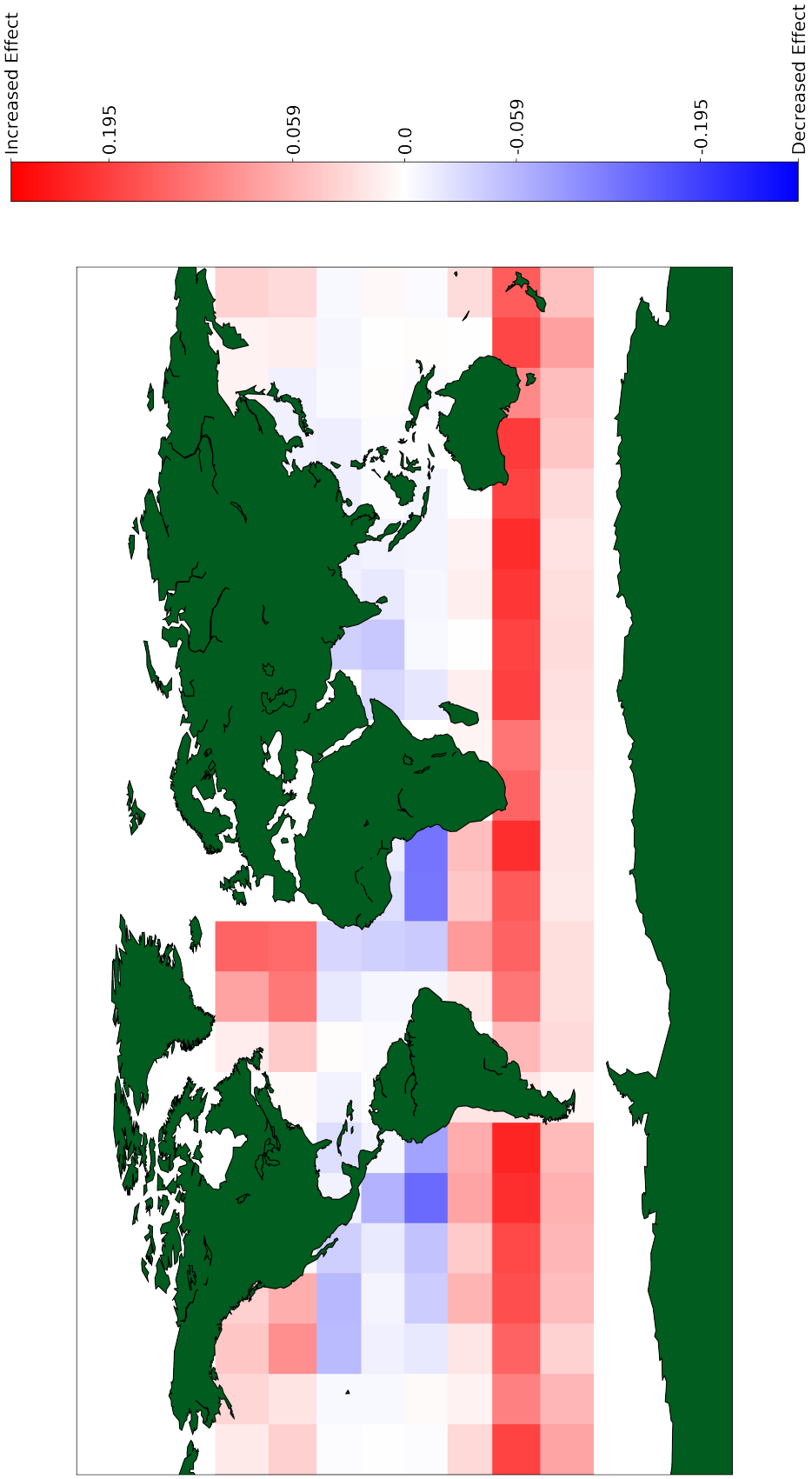

FIGURE 3.14: The forcing sensitivity found within each 15° x 15° region. λ is 5.0 $\frac{\mathrm{Wm}^{-2}}{\ln(\mathrm{AI})}$.

3.3.1 Forcing Sensitivity

There is significant variation in λ when evaluated on a regional 15 x 15 scale (figure 3.14). The weighted sum of the global forcing sensitivity is 5.0 $\frac{\mathrm{Wm}^{-2}}{\ln(\mathrm{AI})}$, although the magnitude and sign varies significantly on a regional scale. The southern ocean dominates the global effect, with the largest positive effects all located at 45°S. The northern hemisphere maximum is located near Iceland in the north Atlantic. The equator and tropical latitudes, from 15 N to 15 S, show an opposite effect globally. A large coherent region of negative sensitivity, representing a warming due to aerosol-cloud interactions, extends throughout the Indian ocean and around the eastern coast of Asia. Although a large portion of the globe shows a negative (warming), the weighted sum is still positive (cooling) due to the frequency and strength in effect of the Southern Ocean's warm clouds.

The pattern of observed variation in magnitude and sign suggest the forcing sensitivity is controlled by regional factors. Global environmental and cloud morphology regimes are able to capture the variation in magnitude, but no cloud regimes displayed a mean warming effect; such effects become readily apparent, however, on regional scales. Clouds near the equator show a propensity to warm the environment due to aerosol-cloud interactions, unlike clouds in the subtropics. Regions of noted similar regimes showed similar sensitivities; the Southeast Pacific and the South Atlantic both showed the same magnitude of effect and are noted to have similar meteorology and cloud states (Mace, 2010).

A warming λ may result from non-linear aerosol-cloud interactions. Within a pristine

environment, aerosol loading will initially impact the cloud significantly. Aerosol limited environments show the greatest response to aerosol loading; cloud growth is limited by the number of CCN (Koren et al., 2014). As aerosol loading continues to increase, the cloud shifts from a regime of aerosol limited to cloud water limited, where there is an excess of aerosol available as CCN. Evaporation and mixing of the cloud layer then reverse the brightening, leading to a negative forcing sensitivity (Chen et al., 2012). The southern hemisphere mid-latitudes show the opposite regime, where aerosol limited regions show a large response to small amounts of aerosol loading. The results presented here are, to the best of our knowledge, the first demonstration that such effects can manifest themselves coherently over large scales like those shown in figure 3.14.

3.3.2 Decomposed Sensitivity

To further explore the source of this spatial variability in aerosol sensitivity, the radiative and cloud adjustment sensitivities are evaluated regionally. The decomposed sensitivity shows similar variation in magnitude and sign as the λ (figure 3.15). The decomposed sensitivity is 5.17 $\frac{\mathrm{Wm}^{-2}}{\ln(\mathrm{AI})}$, 3.4% different compared to the forcing sensitivity from figure 3.14. The decomposed sensitivity displays fewer regions with a warming compared to λ. The equatorial region in the Pacific does not show a negative effect, unlike λ. Only coastal regions directly east of Asia show a negative sensitivity, compared to the large swath of warming throughout the Indian and western Pacific seen in figure 3.14. The equatorial Atlantic shows the same warming signal, but of a lesser magnitude. The Southern Ocean still exhibit the strongest effect, however this extends to further towards the equator than

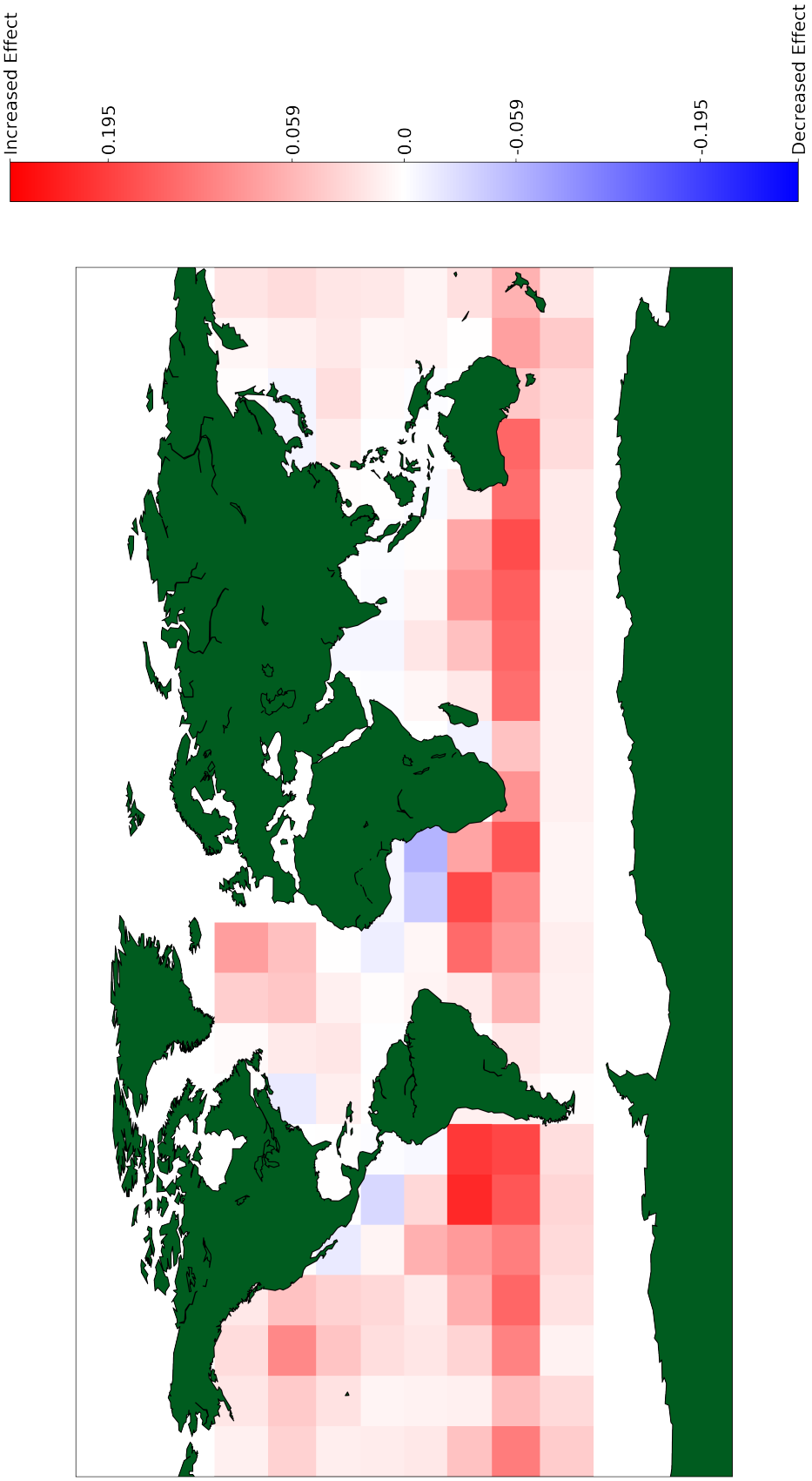

FIGURE 3.15: The decomposed sensitivity found within each 15° x 15° region. Total sum of λ_{RF} and λ_{CA} is 5.16 $\frac{\mathrm{Wm}^{-2}}{\ln(\mathrm{AI})}$.

the regional forcing sensitivity.

The decomposed sensitivity shows very few regions with a warming effect compared to the forcing sensitivity. The magnitude of the southern hemisphere mid-latitudes is significantly less than λ. Because of this, the summed decomposed sensitivity is comparable to the summed forcing sensitivity. However, the regional differences demonstrate λ is not replicated by the decomposed sensitivity. Non-linear aerosol-cloud interactions, demonstrated by the equatorial region of the forcing sensitivity, may not be accurately captured by the decomposition.

3.3.3 Radiative and Cloud Adjustment Sensitivities

The radiative sensitivity contributes almost exactly half of or 2.57 $\frac{\mathrm{Wm}^{-2}}{\ln(\mathrm{AI})}$ to the decomposed sensitivity (figure 3.16). The largest effects are observed throughout the midlatitudes of the Southern Ocean. The global maximum is in the southeastern Pacific. The maximum negative effect is just north of the maximum positive effect, in the tropics off the western coast of South America. There is a slight warming effect throughout tropics globally, except in the eastern Pacific.

The cloud's susceptibility to brighten is highest in the southern oceans (Gryspeerdt et al., 2017). Hemispheric differences in clouds may explain the larger response in the southern vs northern hemisphere (Wood et al., 2002). λ_{RF} in the south Atlantic, equatorial west Pacific, and Indian oceans displays non-linear behavior. The magnitude of λ_{RF} may stay constant at a certain amount of aerosol loading, before reaching a critical value of cloud

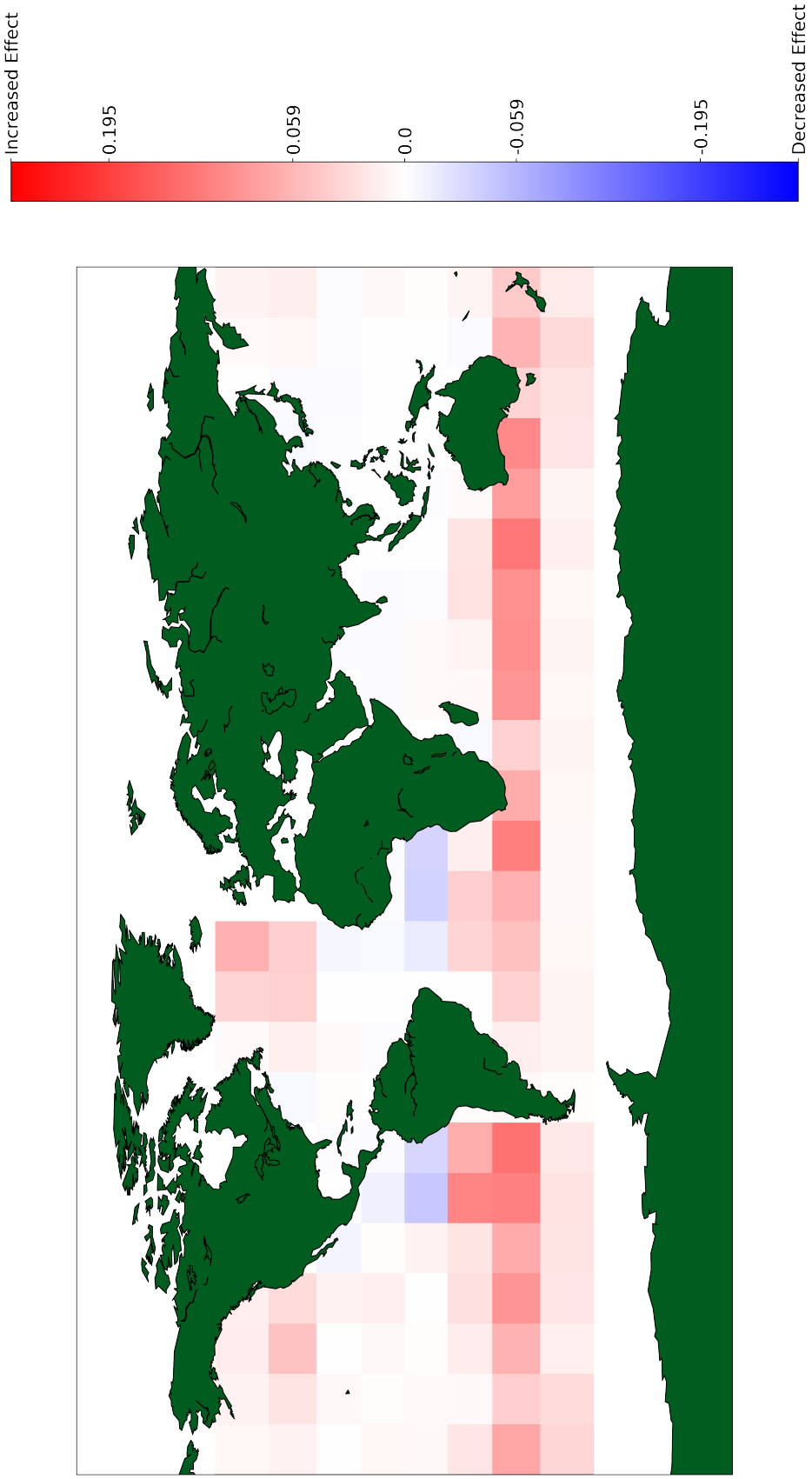

FIGURE 3.16: The radiative sensitivity found within each 15° x 15° region. Total λ_{RF} is 2.57 $\frac{\mathrm{Wm}^{-2}}{\ln(\Delta \mathrm{I})}$.

droplet concentration. After this critical concentration, any further aerosol reverses the effect and the cloud dims (Chandrakar et al., 2016). This non-linear response has been noted by Dagan et al. (2015) on a single cloud scale. The initial cloud drop spectral dispersion may also influence the effect of aerosol loading on cloud brightness, in some cases an increase in aerosol may increase the relative dispersion and decrease albedo (Liu and Daum, 2002). The sign of aerosol impact on albedo therefore reverses in some regions due to cloud dimming. Around 22% of cases experience cloud dimming, similar to other satellite studies looking at aerosol-cloud-albedo interactions (Chen et al., 2015).

Off the southwestern coast of Africa, dimming may be caused by semi-direct effects within the cloud layer due to smoke. Smoke in the cloud layer can darken the cloud. In other regions, the dimming may be a result of extreme aerosol loading leading to cloud breakup (Wood, 2012). The regional variation has been noted in field experiments, where cloud dimming as a result of aerosol was noted in marine stratocumulus clouds (Lu et al., 2007).

Even in regions where clouds bright in response to changes in aerosol loading, λ_{RF} varies regionally. The northern Atlantic and Pacific each show a reduced effects compared to the Southern Ocean. The magnitude of the radiative sensitivity, and cloud brightening, may be controlled regionally by the updraft speed in clouds, which moves aerosol into the activation zone (Hudson and Noble, 2014). Around Australia, where the NASA Goddard GEOS-5 has predicted diminished in-cloud updraft speeds, satellite observations show a reduced radiative sensitivity (Seinfeld et al., 2016). Reducing updraft speeds decrease the number of aerosol activated as CCN, dampening the albedo effect and λ_{RF}. Given their

importance in cloud thermodynamics, role of updraft speeds in the activation of aerosol, and overall aerosol-cloud interactions, must be explored in the future.

The other half of the global decomposed sensitivity is explained by the cloud adjustment sensitivity, which totals 2.6 $\frac{\mathrm{Wm}^{-2}}{\ln(\mathrm{AI})}$ (figure 3.17). Fewer regions experience a negative effect compared to λ_{RF}. The global maximum is in the southeastern Pacific. In the global maximum region, λ_{CA} dominates the decomposed sensitivity.

Off the coast of south Asia, aerosol may work to inhibit cloud growth, decreasing the cloud adjustment effect (Ackerman et al., 2000). Aerosol from soot, dust, and smoke can work to inhibit or erode clouds. Smoke off the coast of Africa may increase cloud top evaporation, decreasing cloud liquid water, and reversing the cloud adjustment effect (Kaufman et al., 2005a). Increased evaporation at the cloud top, forced by increased evaporation from smaller droplets and higher droplet number, is more likely in high aerosol loading environments and can lead to marine stratocumulus breakup (Sandu et al., 2009). The few regions where the λ_{CA} is negative are likely due to evaporation forced by an overload of aerosol extinguishing the cloud deck.

In the tropics, the positive effect may indicate a transition of shallow cumulus to stratocumulus clouds aided by aerosol (Gryspeerdt et al., 2014). Aerosol can aid the transition of closed to open cell stratocumulus; the larger effect in regions of known marine stratocumulus cloud decks (southeast Pacific and south Atlantic) may show invigoration as a sum of the multiple processes that modify cloud extent, like cloud transitions and precipitation, altered by aerosol (Rosenfeld et al., 2006). In marine stratocumulus cloud decks, aerosol

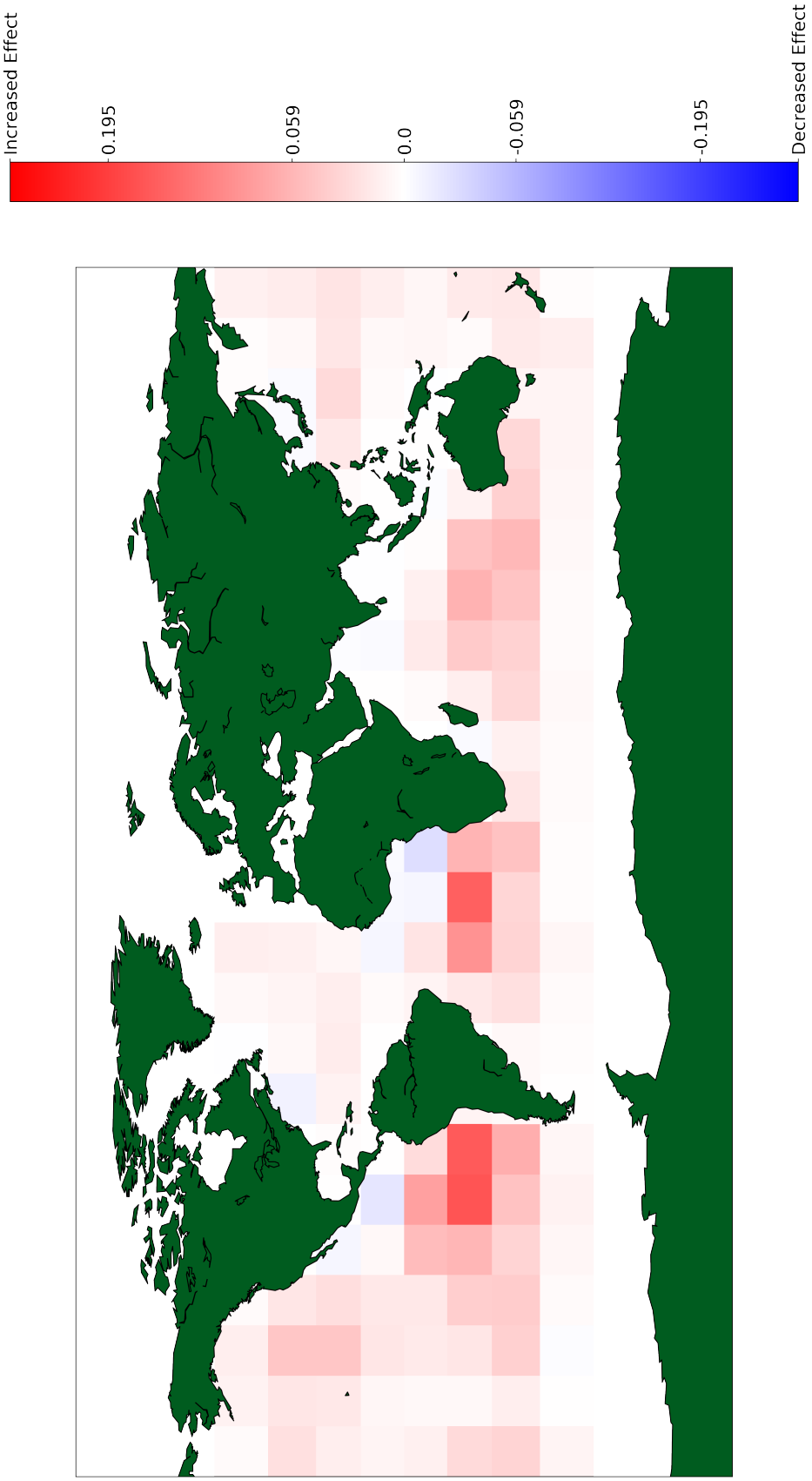

FIGURE 3.17: The cloud adjustment sensitivity found within each 15° x 15° region. Total λ_{CA} is 3.1 $\frac{\mathrm{Wm}^{-2}}{\ln(\mathrm{AI})}$.

may inhibit precipitation, extending cloud lifetime, while altering the local dynamics to transition individual clouds from close to open cell, encouraging cloud growth.

The cloud adjustment sensitivity is regulated not just by regional differences in cloud-aerosol interactions, but by the susceptibility of individual clouds to aerosol forced precipitation modifications. The effect is dampened in many regions due to multiple processes which must collaborate when perturbed by aerosol to produce cloud growth. The decomposition term for cloud adjustments may not encompass all aerosol forced modifications, including the local environment and in cloud dynamics.

Precipitation alters not just the cloud's state, but the environment. Precipitation can stabilize the marine boundary layer, altering the cloud and environment. Within the cloud, precipitation decreases the number of CCN and the cloud liquid water, irreversibly changing the cloud state. The aerosol-cloud-precipitation response is influenced by the initial cloud's state and structure (Christensen and Stephens, 2012). Understanding the relationships between aerosol and the cloud's local environment and precipitation resolve any covarying aerosol effects.

Chapter 4

Conclusions

4.1 Overview

The forcing sensitivity in warm clouds is evaluated using a single linear regression of CERES CRE against ln(AI) and as a sum of its two main components, the radiative and cloud adjustment sensitivities. The forcing and decomposed sensitivities are estimated with global linear regressions, within environmental regimes of EIS and RH, within cloud regimes constrained by LWP, and regionally (table 4.1). λ from the global regression likely overestimates the effect, but can be considered as an upper limit on the effect. The forcing and decomposed sensitivities converged when evaluated within cloud regimes when constrained by LWP. While global separation into regimes sheds light on buffering within the cloud system, not all variation of λ and its components are captured. Regional evaluation of the λ reveals a non-linear relationship between aerosol and cloud forcing.

	Global Regression	Regimes	Regimes with LWP	Regional
λ	14.3	3.12	3.19	5.0
Decomposed λ	9.35	3.81	3.14	5.17
λ_{RF}	3.56	2.01	1.9	2.57
λ_{CA}	5.79	1.8	1.24	2.6

TABLE 4.1: Review of the forcing sensitivity and components evaluated using a single regression (section 3.1), environmental regimes (section 3.3), cloud regimes with LWP constraints (section 3.3.4), and regional regressions.

The decomposition should work to incorporate more terms in order to capture the non-linear variation observed in the regional forcing sensitivity. While global cloud regimes may not be sufficient to quantify the λ, the cloud regime framework can be employed to assess a models ability to capture the mean cloud response to aerosol. Application of this framework regionally represents the best means to quantify the forcing sensitivity and its component. Future work is required to better account for covariability between aerosol-cloud interactions, incorporate more terms into the decomposed sensitivity, and determine the cause of regional variation seen in the all sensitivity estimates. The analysis presented thus far has, however, provided valuable insight into each of the questions posed in section 1.3.

4.2 How large is the shortwave warm cloud forcing sensitivity?

The forcing sensitivity can be evaluated using a linear regression of cloud radiative effect from CERES against ln(AI) from MODIS, however this simple method does not accurately capture the true radiative impact due to aerosol-cloud interactions. Regional

influences, meteorology, cloud state, and nonlinear interactions must be constrained in order to isolate only the effects of aerosol on the cloud's radiative properties. λ is 14.3, 3.12, 3.19, and 5.0 $\frac{\mathrm{Wm}^{-2}}{\ln(\mathrm{AI})}$, varying with constraints on analysis. It was demonstrated that in order to understand current aerosol-cloud interactions, the environment and initial cloud state, both of which can buffer the cloud against aerosol perturbations, and the individual components of the forcing sensitivity must be considered.

Note that the forcing sensitivity estimated here is in units per ln(AI), unlike estimates of the ERFaci from the IPCC and other literature. The true ERFaci quantifies the amplification of the cloud radiative effect from pre-industrial to current times, however measurements of pre-industiral aerosol are far and few between. Using aerosol emissions from models induces another source of error in the computation of ERFaci that we chose to avoid here. Further, it is inconsistent to assume the clouds in current times are comparable to clouds from the pre-industrial era. With lower anthropogenic emissions, the pre-industrial Earth may have been much less cloudy. The role of satellite observations should be to guide models on the current cloud state and place a high end constraint on the ERFaci.

4.3 Can the forcing sensitivity be decomposed into two components, the radiative sensitivity and cloud adjustment sensitivity?

Decomposing the forcing sensitivity allows for the separation of the the two main components. The radiative sensitivity is described by the change in the CSWF from CloudSat with respect to ln(AI), which approximates the modification of the clouds radiation properties like albedo due to aerosol-cloud interactions. The cloud adjustments are defined as the change in the cloud extent with respect to ln(AI). Cloud adjustments include many processes which result in an altered cloud state, however the main effect is on the cloud extent. The decomposed λ, the sum the radiative and cloud adjustment sensitivities, underestimated the forcing sensitivity. Covariability between the radiative and cloud adjustment sensitivities, ignored by our simple decomposition, may have artificially dampened the signal. λ should be described by a sum of parts, not its own single effect. Accurate estimates of the forcing sensitivity will depend on describing all individual cloud processes due to aerosol-cloud interactions. Quantification of the forcing sensitivity must allow for covariability between all aerosol-cloud processes, including precipitation and in cloud dynamics. Our decomposition followed the assumptions of Twomey from 1977 and Albrecht from 1989 which are based on simple cloud models unable to parameterize higher level cloud thermodynamics. Future decompositions should expand the definition of cloud adjustments and account for covariance between the radiative and cloud

adjustment sensitivities.

A key finding from this study is that the global sensitivity of clouds to aerosol is composed almost equally from the radiative and cloud adjustment sensitivities. Not incorporating precipitation interactions may underestimate cloud adjustments. Precipitation suppression may intensify cloud invigoration. The cloud adjustment term must incorporate more aerosol-cloud processes like precipitation suppression and LWP. Evaluating precipitation and covarying cloud extent may explain regional differences in sign and magnitude (figure 3.16). A precipitation term in the cloud adjustments component will demonstrate where precipitation suppression process leads to cloud expansion.

4.4 Does the cloud response depend on regime?

Cloud regimes are the first step to constraining meteorlogical influences on the cloud state. Without accounting for stability, entrainment, and cloud liquid water, any changes in the cloud's radiative properties could be attributed to the environment and not aerosol. The global regressions are known to overestimate both the forcing and radiative sensitivities. A single linear regression fails to capture the proven variation in effect. Both the forcing and decomposed forcing sensitivities decreased when constrained in a cloud regime framework of EIS and RH (figures 3.4, 3.5). Using cloud regimes might impose a lower limit on the forcing sensitivity, and define a minimum mean response of the cloud to aerosol under a range of environmental conditions. The regime framework discerns the role of stability and RH in modulating cloud responses, although variance in effect may still be artificially

ignored even when 25 different cloud regimes are defined. Regional evaluation revealed a warming effect around the equator, however no global cloud regimes exhibited the same signal. Understanding the mean cloud response is one way to optimize parameterization of clouds in global climate models. Cloud regimes should be used to assess the ability of models to represent the environment's role in aerosol-cloud interactions.

When cloud morphology is included in the cloud regime framework, the forcing sensitivity increased while the decomposed forcing sensitivity decreased, converging towards 3.16 $\frac{\mathrm{Wm}^{-2}}{\ln(\mathrm{AI})}$ (section 3.3.4). LWP may be one of the most important cloud properties to constrain. Both the radiative and cloud adjustment sensitivities depend on the cloud liquid water content. Clouds cannot be assumed homogeneous even within regimes of EIS, RH, and LWP. Within limits of 100 $\frac{g}{m^2}$, the impact of a few more $\frac{g}{m^2}$ water can spur the beginning of collision coalescence. Precipitation in the cloud layer can work to lower the cloud top entrainment rate and increase the boundary layer stability (Stevens et al., 1998). A more advanced approach would assess the multivariate regression between LWP, aerosol, and the cloud's radiative properties, which would account for covariation between aerosol-cloud interactions.

4.5 Are there regional responses not captured by cloud regimes?

Regionally, the all sensitivities vary in magnitude and sign (section 3.4). The decomposition holds for regions with a positive forcing sensitivity, indicating the individual

components may not show the same non-linear relationship with aerosol as seen in the forcing sensitivity. The cloud adjustment and radiative sensitivities are negative in a select number of regions, but did not show the same response in the equatorial regions as λ. This may indicate the non-linear relationship between aerosol and a cloud's radiative effect is not captured by the decomposed forcing sensitivity. Including more terms in order to capture the bi-modal relationship is necessary.

The regional scale is best to evaluate and demonstrate the variation in λ. Cloud regimes do not accurately capture the ability for the forcing sensitivity to change sign, from cooling to warming. Even when LWP is added as a regime constraint, no regimes exhibited a negative effect. In order to truly quantify the forcing sensitivity, a regional scale should be used to include all variation.

Chapter 5

Future Work

5.1 Handling of Precipitation

Throughout analysis, precipitating and non-precipitating clouds were grouped together. Precipitating and non-precipitating clouds have different microphysics which may impact aerosol-cloud interactions and cloud adjustment processes. Cloud growth may only be possible in non-precipitating clouds, where scavenging of aerosol is minimized while activation of aerosol as CCN and the delay of collision coalescence is maximized. Separating precipitating and non-precipitating and applying equation 2.4 to find the forcing sensitivity on a regional 15° x 15° scale, λ differs by 13.16 $\frac{\mathrm{Wm}^{-2}}{\ln(\mathrm{AI})}$ between precipitating and non-precipitating clouds (figures 5.1, 5.2). Preliminary results show regionally the precipitating clouds experience a larger negative λ than non-precipitating clouds. The dominance of thin clouds dampens the impact of precipitating clouds when weighted by

occurrence. The regional differences between the precipitating and non-precipitating forcing sensitivity may clarify the patterns of warming and cooling displayed in the regional analysis of λ.

Furthermore, precipitation may adjust both the radiative and cloud adjustment sensitivities magnitude and sign regionally. The individual terms of the forcing sensitivity, λ_{RF} and λ_{CA}, are sensitive to precipitation. The cloud albedo effect, the main effect of the λ_{RF}, may reverse for raining clouds. Cloud adjustments undergo a different set of processes when the cloud is precipitating. Precipitation may alter the distribution of liquid water within a cloud (Lu et al., 2007). Understanding how each component of λ is modulated by precipitation is required to constrain the observed forcing sensitivity and regulate the model parameterization of effects.

5.2 Further Decompositions

The cloud adjustment sensitivity can be further decomposed into two terms, the invigoration of the cloud by aerosol, and the effects of aerosol on precipitation and cloud extent. Albrecht's original cloud lifetime effect, the main component of cloud adjustments, postulated aerosol forced precipitation suppression would be the drive increased cloud liquid water content and cloud extent. If an increase in aerosol does not result in precipitation suppression, but instead precipitation invigoration, there should be no increase in cloud extent. However, aerosol has been found to invigorate or suppress precipitation in clouds depending on the cloud dynamics and environment (Christensen and Stephens, 2012).

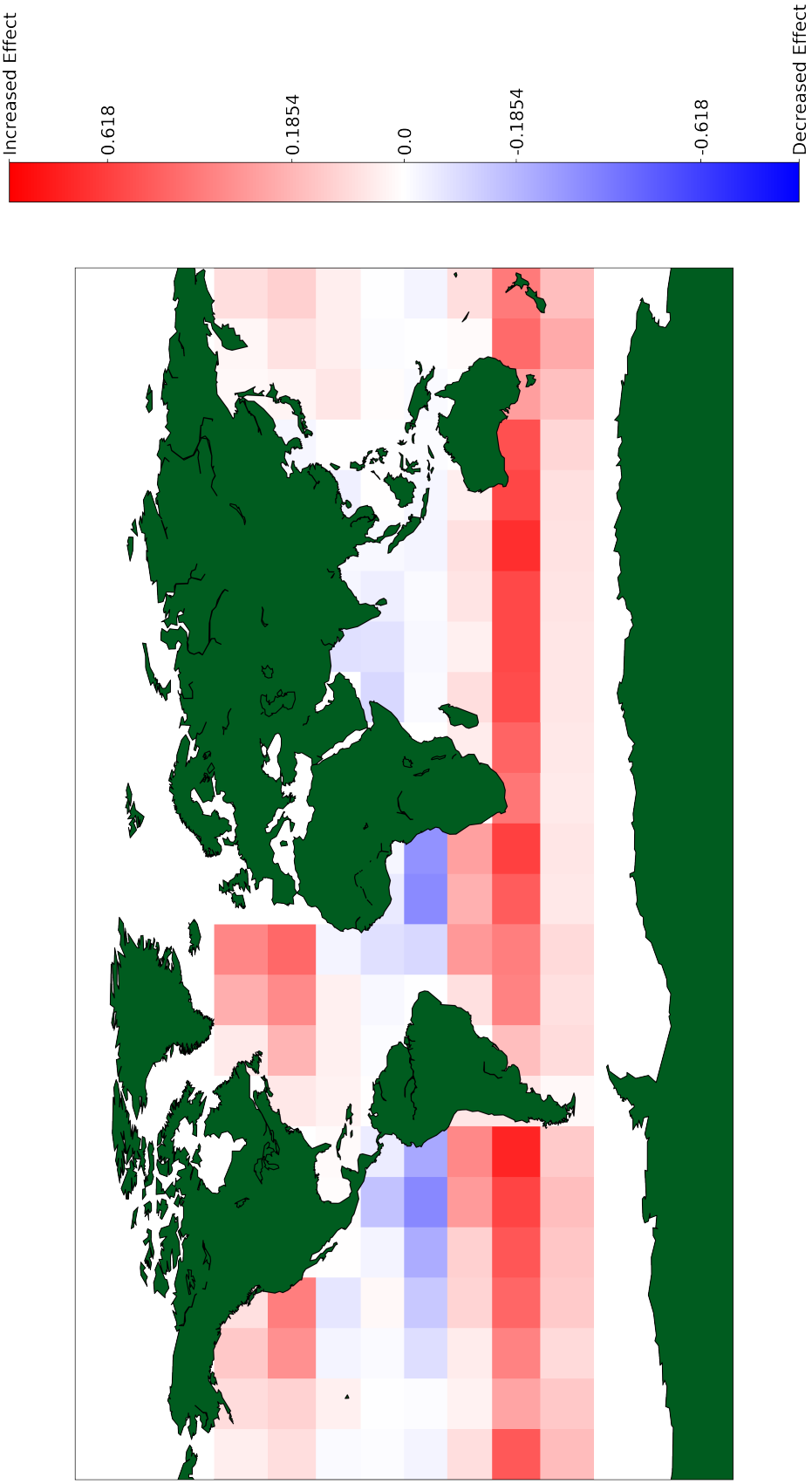

FIGURE 5.1: $\frac{dCERESCRE}{dln(AOD)}$ found within each 15° x 15° region using MODIS AI for non-precipitating clouds. Total λ is 14.54 $\frac{\mathrm{Wm}^{-2}}{\ln(\mathrm{AI})}$.

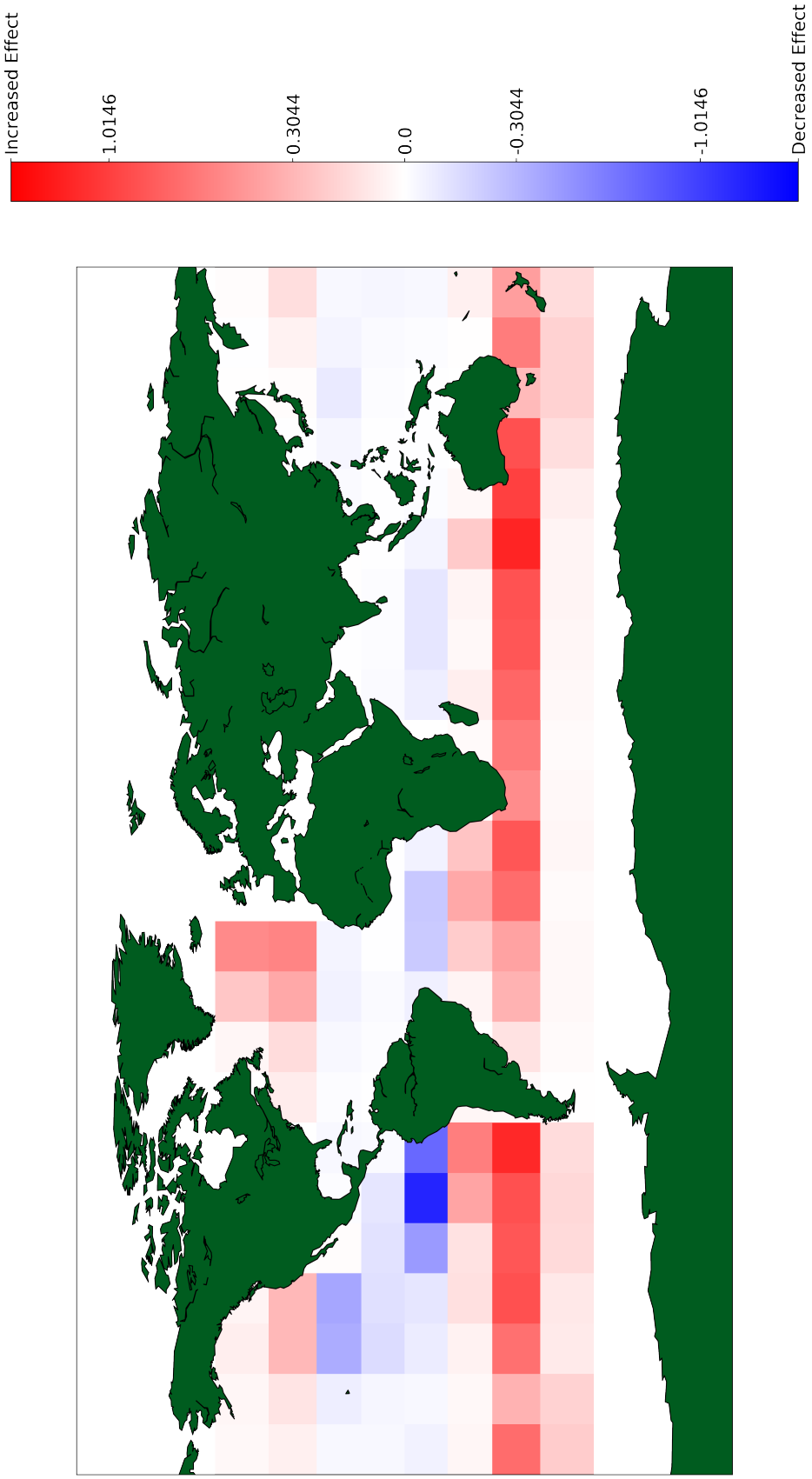

FIGURE 5.2: $\frac{dCERESCRE}{dln(AOD)}$ found within each 15° x 15° region using MODIS AI for precipitating clouds. Total λ is 1.34 $\frac{\mathrm{Wm}^{-2}}{\ln(\mathrm{AI})}$.

Evaluation of each cloud adjustment sensitivity, invigoration of the cloud layer by aerosol and aerosol-precipitation interactions, will further our understanding of the aerosol-cloud interactions and the significance of these to the Earth's climate.

The net forcing sensitivity would be the sum of the shortwave and longwave forcing sensitivities. With CERES and CloudSat longwave forcings, the same analysis can be redone to estimate the longwave forcing sensitivity within regimes and regionally. The net forcing sensitivity could then be combined with modeled estimates of AI to find the ERFaci. The fourth and fifth IPCC reports estimate the longwave ERFaci is insubstantial to total ERFaci estimates (Boucher et al., 2013, Randall et al., 2007). However, aerosol has been shown to invigorate clouds and increase cloud top height, which would lead to a decreased longwave cooling effect (Koren et al., 2014). Thorough analysis of the longwave ERFaci and the decomposed sensitivities may alter or reinforce previously held assumptions.

5.3 Quantifying Environmental Influences

The environment plays a role in modulating cloud processes. Through a systematic study of warm clouds, with thorough investigation into all environmental factors that may influence cloud processes, the strength of environmental controls can be quantified. The cloud state will be further examined by including the warm cloud latent heating product to find the level of maximum heating (Nelson et al., 2016). The level of maximum heating can provide insight into in cloud dynamics such as in cloud updraft speed and the

organization of the rain within the cloud layer (Aubert, 1957). A vertical profile of the atmosphere around clouds will be provided by AIRS, an instrument aboard the NASA A-Train (Schreier et al., 2014). The ability for AIRS to estimate a vertical profile above clouds will be tested and included in analysis if proven accurate against reanalysis. With AIRS observations and MERRA-2 reanalysis, the cloud environment can be parameterized with more than LWP, EIS, and RH, expanding the number of cloud regimes globally. The role of the environment compared to aerosols and cloud state can subsequently be evaluated within the expanded cloud regime framework.

syntonly

Appendix A

Modeled Aerosol Validation

Satellite observations of aerosol may be affected by cloud contamination within the observed pixel while satellite observations of cloud albedo may be contaminated by overlying absorbing aerosols. Although these contamination induced errors may be insignificant with the large sampling size, the robustness of all observed signals should be tested to verify all results Kaufman et al. (2005b). To validate the signal seen in all global estimates of the forcing and decomposed forcing sensitivities, the analysis is repeated using modeled sulfate aerosol optical depth from the Global Earth system Monitoring using Space and in-situ data project (MACC) Hollingsworth et al. (2008). Aerosol optical depth and aerosol index are both correlated to the concentration within the atmosphere, however aerosol index is weighted to the size of the particle. All estimates of forcing will be in $\frac{W}{m^2 ln(AOD)}$, compared to $\frac{W}{m^2 ln(AI)}$ used during our analysis, and be amplified by a factor of 10.

A.1 Forcing sensitivity

Assessing λ regionally using the modeled MACC sulfate AOD, the MODIS AI and MACC SU forcing sensitivities agree in regions where the MODIS λ showed cooling, but disagree in the equatorial region where the MODIS λ indicated a warming effect (figure A.1). The MODIS λ shows a swath of negative effect along equatorial region, while the MACC only shows a few regions with a negative effect. Interestingly, the few regions where MACC is negative agree with the decomposed forcing sensitivity map. The total SU AOD forcing sensitivity is 27.07 $\frac{W}{m^2 ln(AOD)}$. The southern oceans show a maximum region along the mid-latitudes, very similar to both the forcing and decomposed forcing sensitivities.

A.2 Decomposed ERFaci

The MACC decomposed λ underestimates the effect compared to the MACC λ in all regions (figure A.2). The MACC SU radiative sensitivity shows the same global maximum off the coast of South America, similar to the MODIS radiative sensitivity (MACC SU λ_{RF} not shown). The cloud adjustment sensitivity shows a scattered pattern, inconsistent with λ_{CA} when evaluated with MODIS AI (figure A.4, section 3.4.3). λ_{CA}, when evaluated with MACC SU, drops from comprising 50% of the decomposed λ to 33% (not shown). If the cloud adjustment term was corrected to be the same magnitude as the MACC SU λ_{RF}, the decomposed λ would increase from 11.21 to 16.31 $\frac{W}{m^2 ln(AOD)}$ and reduce the error between the MACC λ and decomposed λ from 59% to 40%. AOD is weighted towards larger particles and is only weakly correlated with cloud droplet concentration.

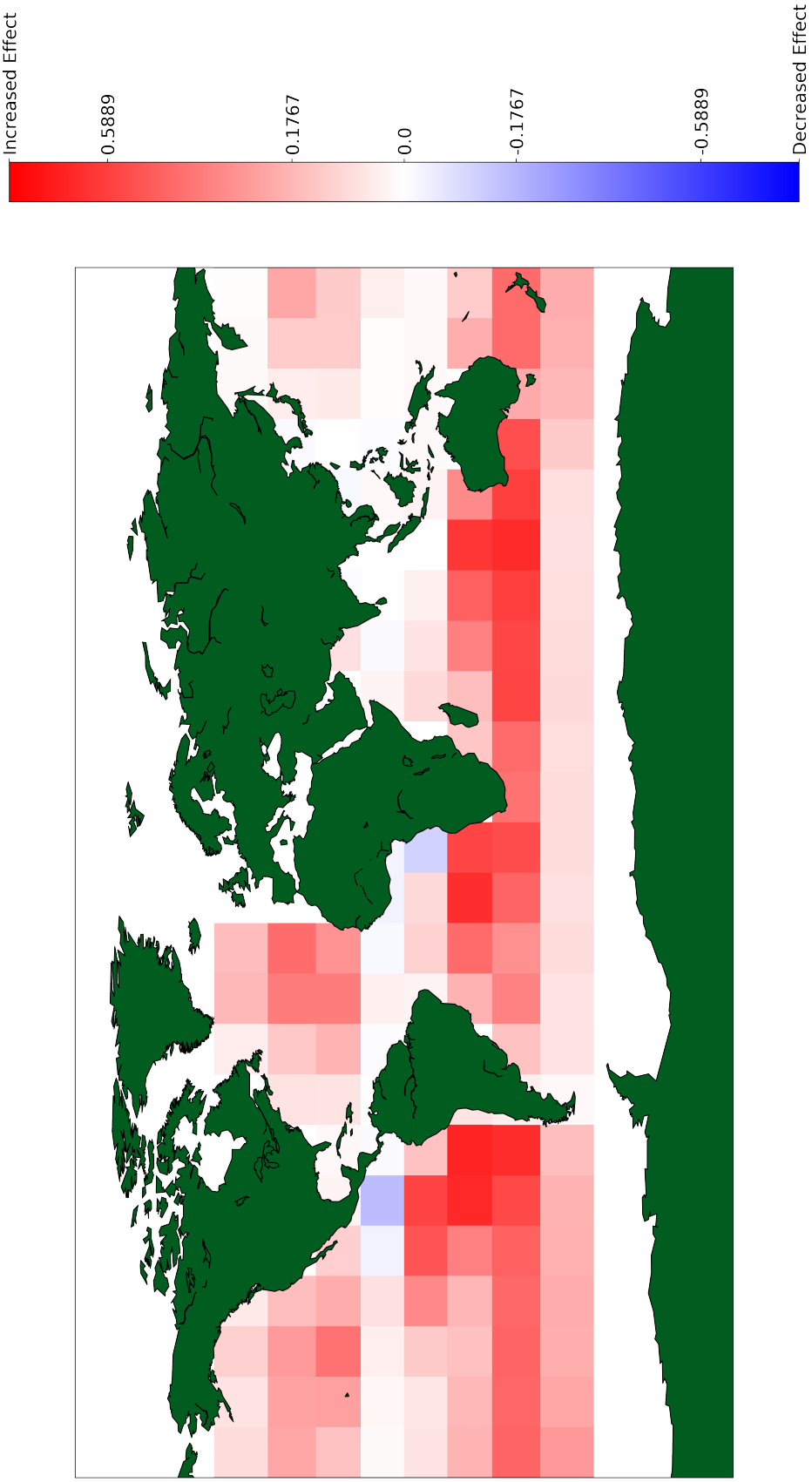

FIGURE A.1: $\frac{dCERESCRE}{dln(AOD)}$ found within each 15° x 15° region using MACC sulfate AOD. Total λ is 27.07 $\frac{W}{m^2 ln(AOD)}$.

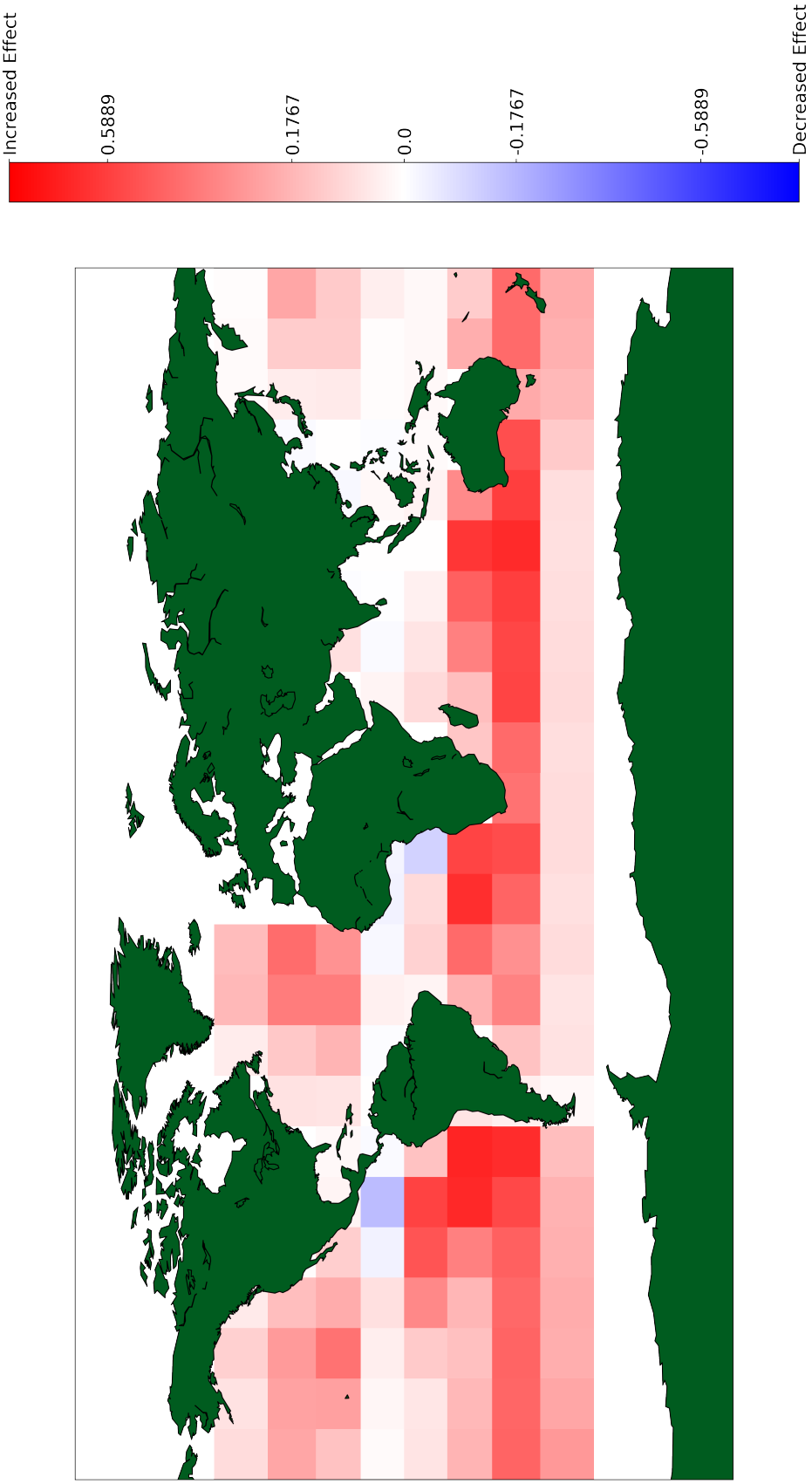

FIGURE A.2: From equation 2.5, the decomposed ERFaci found within each 15° x 15° region using MACC sulfate AOD. Total RFaci is 8.15 $\frac{W}{m^2 ln(AOD)}$.

Compared to AI, AOD is not representative of of aerosol within the cloud layer and will underestimate the effect of all forcing sensitivity components Gryspeerdt et al. (2017). The weak relationship between AOD and cloud droplet concentration may be the source of error between the forcing and decomposed forcing sensitivities. The components of the forcing sensitivity assume aerosol is available as a CCN. This assumption fails if the aerosol is too large to act as an available CCN. The degradation of this relationship may result in a weaker effect for higher values of ln(AI), corresponding to larger particles, as seen in sections 3.1 and 3.2.

Bibliography

Ackerman, A. S., M. P. Kirkpatrick, D. E. Stevens, and O. B. Toon, 2004: The impact of humidity above stratiform clouds on indirect aerosol climate forcing. *Nature*, **432**, 1014–1017.

Ackerman, A. S., O. Toon, D. Stevens, A. Heymsfield, V. Ramanathan, and E. Welton, 2000: Reduction of tropical cloudiness by soot. *Science*, **288**, 1042–1047.

Albrecht, B., 1989: Aerosols, cloud microphysics, and fractional cloudiness. *Science*, **245**, 1227–1230.

Altaratz, O., I. Koren, L. Remer, and E. Hirsch, 2014: Review: Cloud invigoration by aerosols—coupling between microphysics and dynamics. *Atmospheric Research*, **140**, 38–60.

Andersen, H. and J. Cermak, 2015: How thermodynamic environments control stratocumulus microphysics and interactions with aerosols. *Environmental Research Letters*, **10**, 024004.

Aubert, E. J., 1957: On the release of latent heat as a factor in large scale atmospheric motions. *Journal of Meteorology*, **14**, 527–542.

Bender, F. A.-M., A. Engström, and J. Karlsson, 2016: Factors controlling cloud albedo in marine subtropical stratocumulus regions in climate models and satellite observations. *Journal of Climate*, **29**, 3559–3587.

Bony, S. and J.-L. Dufresne, 2005: Marine boundary layer clouds at the heart of tropical cloud feedback uncertainties in climate models. *Geophysical Research Letters*, **32**.

Bosilovich, M. G., S. Akella, L. Coy, R. Cullather, C. Draper, R. Gelaro, R. Kovach, Q. Liu, A. Molod, P. Norris, et al., 2015: Merra-2: Initial evaluation of the climate. *Series on Global Modeling and Data Assimilation, NASA/TM*, **104606**.

Boucher, O., D. Randall, P. Artaxo, C. Bretherton, G. Feingold, P. Forster, V.-M. Kerminen, Y. Kondo, H. Liao, U. Lohmann, et al., 2013: Clouds and aerosols. *Climate change 2013: the physical science basis. Contribution of Working Group I to the Fifth Assessment Report of the Intergovernmental Panel on Climate Change*, Cambridge University Press, 571–657.

Carslaw, K., L. Lee, C. Reddington, K. Pringle, A. Rap, P. Forster, G. Mann, D. Spracklen, M. Woodhouse, L. Regayre, et al., 2013: Large contribution of natural aerosols to uncertainty in indirect forcing. *Nature*, **503**, 67–71.

Carslaw, K. S., H. Gordon, D. S. Hamilton, J. S. Johnson, L. A. Regayre, M. Yoshioka, and K. J. Pringle, 2017: Aerosols in the pre-industrial atmosphere. *Current Climate Change Reports*, **3**, 1–15.

Chandrakar, K. K., W. Cantrell, K. Chang, D. Ciochetto, D. Niedermeier, M. Ovchinnikov, R. A. Shaw, and F. Yang, 2016: Aerosol indirect effect from turbulence-induced broadening of cloud-droplet size distributions. *Proceedings of the National Academy of Sciences*, **113**, 14243–14248.

Chen, Y.-C., M. Christensen, L. Xue, A. Sorooshian, G. Stephens, R. Rasmussen, and J. Seinfeld, 2012: Occurrence of lower cloud albedo in ship tracks. *Atmospheric Chemistry and Physics*, **12**, 8223–8235.

Chen, Y.-C., M. W. Christensen, D. J. Diner, and M. J. Garay, 2015: Aerosol-cloud interactions in ship tracks using terra modis/misr. *Journal of Geophysical Research: Atmospheres*, **120**, 2819–2833.

Chen, Y.-C., M. W. Christensen, G. L. Stephens, and J. H. Seinfeld, 2014: Satellite-based estimate of global aerosol-cloud radiative forcing by marine warm clouds. *Nature Geoscience*, **7**, 643–646.

Christensen, M. W., Y.-C. Chen, and G. L. Stephens, 2016: Aerosol indirect effect dictated by liquid clouds. *Journal of Geophysical Research: Atmospheres*.

Christensen, M. W. and G. L. Stephens, 2011: Microphysical and macrophysical responses of marine stratocumulus polluted by underlying ships: Evidence of cloud deepening. *Journal of Geophysical Research: Atmospheres*, **116**.

— 2012: Microphysical and macrophysical responses of marine stratocumulus polluted by underlying ships: 2. impacts of haze on precipitating clouds. *Journal of Geophysical Research: Atmospheres*, **117**.

Dagan, G., I. Koren, and O. Altaratz, 2015: Competition between core and periphery-based processes in warm convective clouds–from invigoration to suppression. *Atmospheric Chemistry and Physics*, **15**, 2749–2760.

Dagan, G., I. Koren, O. Altaratz, and R. H. Heiblum, 2017: Time-dependent, non-monotonic response of warm convective cloud fields to changes in aerosol loading. *Atmospheric Chemistry and Physics*, **17**, 7435–7444.

Engström, A., F. A.-M. Bender, and J. Karlsson, 2014: Improved representation of marine stratocumulus cloud shortwave radiative properties in the cmip5 climate models. *Journal of Climate*, **27**, 6175–6188.

Feingold, G., A. McComiskey, T. Yamaguchi, J. S. Johnson, K. S. Carslaw, and K. S. Schmidt, 2016: New approaches to quantifying aerosol influence on the cloud radiative effect. *Proceedings of the National Academy of Sciences*, **113**, 5812–5819.

Forster, P., V. Ramaswamy, P. Artaxo, T. Berntsen, R. Betts, D. W. Fahey, J. Haywood, J. Lean, D. C. Lowe, G. Myhre, et al., 2007: Changes in atmospheric constituents and in radiative forcing. chapter 2. *Climate Change 2007. The Physical Science Basis*.

Ghan, S., M. Wang, S. Zhang, S. Ferrachat, A. Gettelman, J. Griesfeller, Z. Kipling, U. Lohmann, H. Morrison, D. Neubauer, et al., 2016: Challenges in constraining anthropogenic aerosol effects on cloud radiative forcing using present-day spatiotemporal variability. *Proceedings of the National Academy of Sciences*, **113**, 5804–5811.

Goren, T. and D. Rosenfeld, 2015: Extensive closed cell marine stratocumulus downwind of europe—a large aerosol cloud mediated radiative effect or forcing? *Journal of Geophysical Research: Atmospheres*, **120**, 6098–6116.

Grandey, B. and P. Stier, 2010: A critical look at spatial scale choices in satellite-based aerosol indirect effect studies. *Atmospheric Chemistry and Physics*, **10**, 11459–11470.

Gryspeerdt, E., J. Quaas, and N. Bellouin, 2016: Constraining the aerosol influence on cloud fraction. *Journal of Geophysical Research: Atmospheres*, **121**, 3566–3583.

Gryspeerdt, E., J. Quaas, S. Ferrachat, A. Gettelman, S. Ghan, U. Lohmann, H. Morrison, D. Neubauer, D. G. Partridge, P. Stier, et al., 2017: Constraining the instantaneous aerosol influence on cloud albedo. *Proceedings of the National Academy of Sciences*, **114**, 4899–4904.

Gryspeerdt, E., P. Stier, and D. Partridge, 2014: Satellite observations of cloud regime development: the role of aerosol processes. *Atmospheric Chemistry and Physics*, **14**, 1141–1158.

Guo, Z., M. Wang, Y. Qian, V. E. Larson, S. Ghan, M. Ovchinnikov, P. A. Bogenschutz, C. Zhao, G. Lin, and T. Zhou, 2014: A sensitivity analysis of cloud properties to clubb parameters in the single-column community atmosphere model (scam5). *Journal of Advances in Modeling Earth Systems*, **6**, 829–858.

Hahn, C. and S. Warren, 2007: A gridded climatology of clouds over land (1971-96) and ocean (1954-97 from surface observations worldwide. Technical report, Office of Biological and Environmental Research.

Hirsch, E., I. Koren, O. Altaratz, Z. Levin, and E. Agassi, 2017: Enhanced humidity pockets originating in the mid boundary layer as a mechanism of cloud formation below the lifting condensation level. *Environmental Research Letters*, **12**, 024020.

Hollingsworth, A., R. Engelen, A. Benedetti, A. Dethof, J. Flemming, J. Kaiser, J. Morcrette, A. Simmons, C. Textor, O. Boucher, et al., 2008: Toward a monitoring and forecasting system for atmospheric composition: The gems project. *Bulletin of the American Meteorological Society*, **89**, 1147–1164.

Hudson, J. G. and S. Noble, 2014: Ccn and vertical velocity influences on droplet concentrations and supersaturations in clean and polluted stratus clouds. *Journal of the Atmospheric Sciences*, **71**, 312–331.

Jiang, H., H. Xue, A. Teller, G. Feingold, and Z. Levin, 2006: Aerosol effects on the lifetime of shallow cumulus. *Geophysical Research Letters*, **33**.

Kaufman, Y. J., I. Koren, L. A. Remer, D. Rosenfeld, and Y. Rudich, 2005a: The effect of smoke, dust, and pollution aerosol on shallow cloud development over the atlantic ocean. *Proceedings of the National Academy of Sciences of the United States of America*, **102**, 11207–11212.

Kaufman, Y. J., L. A. Remer, D. Tanré, R.-R. Li, R. Kleidman, S. Mattoo, R. C. Levy, T. F. Eck, B. N. Holben, C. Ichoku, et al., 2005b: A critical examination of the residual cloud contamination and diurnal sampling effects on modis estimates of aerosol over ocean. *IEEE Transactions on Geoscience and Remote Sensing*, **43**, 2886–2897.

Koren, I., G. Dagan, and O. Altaratz, 2014: From aerosol-limited to invigoration of warm convective clouds. *Science*, **344**, 1143–1146.

Lebsock, M. D., G. L. Stephens, and C. Kummerow, 2008: Multisensor satellite observations of aerosol effects on warm clouds. *Journal of Geophysical Research: Atmospheres*, **113**.

Liu, Y. and P. H. Daum, 2002: Anthropogenic aerosols: Indirect warming effect from dispersion forcing. *Nature*, **419**, 580–581.

Loeb, N., 2014: Ceres ebaf edition 2.8 data quality summary. Technical report, NASA.

Lohmann, U. and J. Feichter, 2005: Global indirect aerosol effects: a review. *Atmospheric Chemistry and Physics*, **5**, 715–737.

Lu, M.-L., W. C. Conant, H. H. Jonsson, V. Varutbangkul, R. C. Flagan, and J. H. Seinfeld, 2007: The marine stratus/stratocumulus experiment (mase): Aerosol-cloud relationships in marine stratocumulus. *Journal of Geophysical Research: Atmospheres*, **112**.

Lu, M.-L. and J. H. Seinfeld, 2005: Study of the aerosol indirect effect by large-eddy simulation of marine stratocumulus. *Journal of the atmospheric sciences*, **62**, 3909–3932.

Ma, X., F. Yu, and J. Quaas, 2014: Reassessment of satellite-based estimate of aerosol climate forcing. *Journal of Geophysical Research: Atmospheres*, **119**.

Mace, G. G., 2010: Cloud properties and radiative forcing over the maritime storm tracks of the southern ocean and north atlantic derived from a-train. *Journal of Geophysical Research: Atmospheres*, **115**.

McCoy, D., F.-M. Bender, J. Mohrmann, D. Hartmann, R. Wood, and D. Grosvenor, 2017: The global aerosol-cloud first indirect effect estimated using modis, merra, and aerocom. *Journal of Geophysical Research: Atmospheres*, **122**, 1779–1796.

Nelson, E. L., T. S. L'Ecuyer, S. M. Saleeby, W. Berg, S. R. Herbener, and S. C. van den Heever, 2016: Toward an algorithm for estimating latent heat release in warm rain systems. *Journal of Atmospheric and Oceanic Technology*, **33**, 1309–1329.

Painemal, D. and P. Zuidema, 2011: Assessment of modis cloud effective radius and optical thickness retrievals over the southeast pacific with vocals-rex in situ measurements. *Journal of Geophysical Research: Atmospheres*, **116**.

— 2013: The first aerosol indirect effect quantified through airborne remote sensing during vocals-rex. *Atmospheric Chemistry and Physics*, **13**, 917–931.

Penner, J. E., M. Andreae, H. Annegarn, L. Barrie, J. Feichter, D. Hegg, A. Jayaraman, R. Leaitch, D. Murphy, J. Nganga, et al., 2001: Aerosols, their direct and indirect effects. *Climate Change 2001: The Scientific Basis. Contribution of Working Group I to the Third Assessment Report of the Intergovernmental Panel on Climate Change*, Cambridge University Press, 289–348.

Quaas, J., Y. Ming, S. Menon, T. Takemura, M. Wang, J. E. Penner, A. Gettelman, U. Lohmann, N. Bellouin, O. Boucher, et al., 2009: Aerosol indirect effects–general circulation model intercomparison and evaluation with satellite data. *Atmospheric Chemistry and Physics*, **9**, 8697–8717.

Randall, D. A., R. A. Wood, S. Bony, R. Colman, T. Fichefet, J. Fyfe, V. Kattsov, A. Pitman, J. Shukla, J. Srinivasan, et al., 2007: Climate models and their evaluation. *Climate change 2007: The physical science basis. Contribution of Working Group I to the Fourth Assessment Report of the IPCC (FAR)*, Cambridge University Press, 589–662.

Rosenfeld, D., Y. Kaufman, and I. Koren, 2006: Switching cloud cover and dynamical regimes from open to closed benard cells in response to the suppression of precipitation by aerosols. *Atmospheric Chemistry and Physics*, **6**, 2503–2511.

Rosenfeld, D., U. Lohmann, G. B. Raga, C. D. O'Dowd, M. Kulmala, S. Fuzzi, A. Reissell, and M. O. Andreae, 2008: Flood or drought: how do aerosols affect precipitation? *science*, **321**, 1309–1313.

Sandu, I., J.-L. Brenguier, O. Geoffroy, O. Thouron, and V. Masson, 2008: Aerosol impacts on the diurnal cycle of marine stratocumulus. *Journal of the Atmospheric Sciences*, **65**, 2705–2718.

Sandu, I., J.-L. Brenguier, O. Thouron, and B. Stevens, 2009: How important is the vertical structure for the representation of aerosol impacts on the diurnal cycle of marine stratocumulus? *Atmospheric Chemistry and Physics*, **9**, 4039–4052.

Schreier, M., B. Kahn, K. Sušelj, J. Karlsson, S. Ou, Q. Yue, and S. Nasiri, 2014: Atmospheric parameters in a subtropical cloud regime transition derived by airs and modis: observed statistical variability compared to era-interim. *Atmospheric Chemistry and Physics*, **14**, 3573–3587.

Schreier, M., H. Mannstein, V. Eyring, and H. Bovensmann, 2007: Global ship track distribution and radiative forcing from 1 year of aatsr data. *Geophysical Research Letters*, **34**.

Schuster, G. L., O. Dubovik, and B. N. Holben, 2006: Angstrom exponent and bimodal aerosol size distributions. *Journal of Geophysical Research: Atmospheres*, **111**.

Seinfeld, J. H., C. Bretherton, K. S. Carslaw, H. Coe, P. J. DeMott, E. J. Dunlea, G. Feingold, S. Ghan, A. B. Guenther, R. Kahn, et al., 2016: Improving our fundamental understanding of the role of aerosol- cloud interactions in the climate system. *Proceedings of the National Academy of Sciences*, **113**, 5781–5790.

Small, J. D., P. Y. Chuang, G. Feingold, and H. Jiang, 2009: Can aerosol decrease cloud lifetime? *Geophysical Research Letters*, **36**.

Stevens, B., W. R. Cotton, G. Feingold, and C.-H. Moeng, 1998: Large-eddy simulations of strongly precipitating, shallow, stratocumulus-topped boundary layers. *Journal of the atmospheric sciences*, **55**, 3616–3638.

Stevens, B. and G. Feingold, 2009: Untangling aerosol effects on clouds and precipitation in a buffered system. *Nature*, **461**, 607–613.

Stevens, B. and A. Seifert, 2008: Understanding macrophysical outcomes of microphysical choices in simulations of shallow cumulus convection. *Journal of the Meteorological Society of Japan. Ser. II*, **86**, 143–162.

Tanelli, S., S. L. Durden, E. Im, K. S. Pak, D. G. Reinke, P. Partain, J. M. Haynes, and R. T. Marchand, 2008: Cloudsat's cloud profiling radar after two years in orbit: Performance, calibration, and processing. *IEEE Transactions on Geoscience and Remote Sensing*, **46**, 3560–3573.

Twomey, S., 1977: The influence of pollution on the shortwave albedo of clouds. *Journal of the Atmospheric Sciences*, **34**, 1149–1152.

Wang, M., S. Ghan, X. Liu, T. S. L'Ecuyer, K. Zhang, H. Morrison, M. Ovchinnikov, R. Easter, R. Marchand, D. Chand, et al., 2012: Constraining cloud lifetime effects of aerosols using a-train satellite observations. *Geophysical Research Letters*, **39**.

Wang, M., S. Ghan, M. Ovchinnikov, X. Liu, R. Easter, E. Kassianov, Y. Qian, and H. Morrison, 2011: Aerosol indirect effects in a multi-scale aerosol-climate model pnnl-mmf. *Atmospheric Chemistry and Physics*, **11**, 5431.

Wood, R., 2007: Cancellation of aerosol indirect effects in marine stratocumulus through cloud thinning. *Journal of the atmospheric sciences*, **64**, 2657–2669.

— 2012: Stratocumulus clouds. *Monthly Weather Review*, **140**, 2373–2423.

Wood, R., C. Bretherton, and D. Hartmann, 2002: Diurnal cycle of liquid water path over the subtropical and tropical oceans. *Geophysical Research Letters*, **29**.

Wood, R. and C. S. Bretherton, 2004: Boundary layer depth, entrainment, and decoupling in the cloud-capped subtropical and tropical marine boundary layer. *Journal of climate*, **17**, 3576–3588.

— 2006: On the relationship between stratiform low cloud cover and lower-tropospheric stability. *Journal of climate*, **19**, 6425–6432.

Wood, R., M. P. Jensen, J. Wang, C. S. Bretherton, S. M. Burrows, A. D. Del Genio, A. M. Fridlind, S. J. Ghan, V. P. Ghate, P. Kollias, et al., 2016: Planning the next

decade of coordinated research to better understand and simulate marine low clouds. *Bulletin of the American Meteorological Society*, **97**, 1699–1702.